

Review

Radar Interferometry for Urban Infrastructure Stability Monitoring: From Techniques to Applications

Songbo Wu ¹, Bochen Zhang ², Xiaoli Ding ^{1,*}, Lei Zhang ³, Zhijie Zhang ^{1,4} and Zeyu Zhang ¹

¹ Department of Land Surveying and Geo-Informatics, Research Institute for Land and Space, The Hong Kong Polytechnic University, Hong Kong 999077, China; song.bo.wu@connect.polyu.hk (S.W.); 2022126054@chd.edu.cn (Z.Z.); ze-yu.zhang@connect.polyu.hk (Z.Z.)

² MNR Key Laboratory for Geo-Environmental Monitoring of Great Bay Area, College of Civil and Transportation Engineering, Shenzhen University, Shenzhen 518060, China; bochen.zh@gmail.com

³ College of Surveying and Geo-Informatics, Tongji University, Shanghai 200092, China; lslzhang@tongji.edu.cn

⁴ School of Geological Engineering and Geomatics, Chang'an University, Xi'an 710054, China

* Correspondence: xl.ding@polyu.edu.hk

Abstract: Urban infrastructure is an important part of supporting the daily operation of a city. The stability of infrastructure is subject to various deformations related to disasters, engineering activities, and loadings. Regular monitoring of such deformations is critical to identify potential risks to infrastructure and take timely remedial actions. Among the advanced geodetic technologies available, radar interferometry has been widely used for infrastructure stability monitoring due to its extensive coverage, high spatial resolution, and accurate deformation measurements. Specifically, spaceborne InSAR and ground-based radar interferometry have become increasingly utilized in this field. This paper presents a comprehensive review of both technologies for monitoring urban infrastructures. The review begins by introducing the principles and their technical development. Then, a bibliometric analysis and the major advancements and applications of urban infrastructure monitoring are introduced. Finally, the paper identifies several challenges associated with those two radar interferometry technologies for monitoring urban infrastructure. These challenges include the inconsistent in the distribution of selected measurements from different methods, obstacles arising from rapid urbanization and geometric distortion, specialized monitoring techniques for distinct urban features, long-term deformation monitoring, and accurate interpretation of deformation. It is important to carry out further research to tackle these challenges effectively.

Keywords: infrastructure stability monitoring; deformation monitoring; radar interferometry; InSAR; GBRI



Citation: Wu, S.; Zhang, B.; Ding, X.; Zhang, L.; Zhang, Z.; Zhang, Z. Radar Interferometry for Urban Infrastructure Stability Monitoring: From Techniques to Applications. *Sustainability* **2023**, *15*, 14654. <https://doi.org/10.3390/su151914654>

Academic Editor: Vincenzo Barrile

Received: 15 August 2023

Revised: 8 September 2023

Accepted: 28 September 2023

Published: 9 October 2023



Copyright: © 2023 by the authors. Licensee MDPI, Basel, Switzerland. This article is an open access article distributed under the terms and conditions of the Creative Commons Attribution (CC BY) license (<https://creativecommons.org/licenses/by/4.0/>).

1. Introduction

Urban infrastructures, including buildings, transit systems, power lines, and water systems are a vital part of a city that supports the daily operation of the city. These infrastructures can become vulnerable due to issues such as construction flaws [1], wear and tear [2], disturbance from nearby construction projects, and various geohazards such as earthquakes, landslides, floods, and ground subsidence [3]. These issues may lead to various forms of structural deformations and incidents such as building collapses [4], sinkholes [5], and dam failures [6]. It is essential to regularly monitor the stability conditions of urban infrastructures to identify any potential risks and take timely remedial actions.

Monitoring the deformation of urban infrastructures is a key part of structural stability monitoring [7]. Various technologies have been developed for monitoring deformations of infrastructures, including in situ sensor-based technologies such as displacement transducers, accelerometers, and fiber sensors; and geodetic technologies such as robotic total stations and global navigation satellite systems (GNSS) [8]. However, due to the high cost involved and operational constraints, these technologies can only collect data from small

portions of an infrastructure or a very limited number of sample points. The advances in remote sensing technology over recent decades, particularly in radar interferometry, have substantially improved the capability of the technology in detecting deformations of ground and infrastructures [9–12]. Radar interferometry technology, especially the spaceborne InSAR (interferometric synthetic aperture radar), has been extensively employed to detect deformations with unprecedented high spatial resolution and measurement accuracy [13–15]. With the advent of the new generation of high spatial resolution and of shorter revisit time spaceborne SAR sensors, the technology has gained even more attention in recent years for infrastructure monitoring at both regional and individual infrastructure levels [16–19]. Furthermore, ground-based radar interferometry (GBRI) has also proven to be very useful for studying infrastructure deformations and has been applied to investigate a range of urban structures such as urban slopes [20,21] and individual structures [22]. Along with the advances in both the sensors and techniques, radar interferometry poses to offer more and wider applications in infrastructure stability monitoring albeit still with some stiff technical challenges [23,24].

This paper aims to provide a comprehensive review of the applications of radar interferometry technology in urban infrastructure stability monitoring, with a focus on spaceborne InSAR and GBRI. Section 2 briefly introduces the principal of radar interferometry and their developments. Section 3 presents a bibliometric analysis. Section 4 analyses the recent advances and applications. The limitations of the technology in such applications and opportunities for future research are discussed in Section 5. Finally, Section 6 provides some conclusions from this study.

2. Radar Interferometry

2.1. Principle

Radar is an active remote sensing technology, as shown in Figure 1, that transmits radio pulses along the line-of-sight (LOS) to detect and measure the range of targets through analyzing the reflected signal [25].

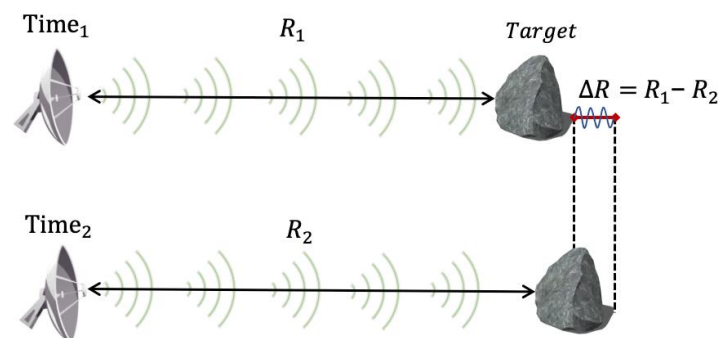


Figure 1. A radar sensor measures the ranges to a target at different times.

The synthetic aperture radar (SAR) is an imaging technique using a moving platform with a radar antenna to capture high-resolution radar images. SAR images, S , are recorded as complex values that can be expressed as Equation (1), represented by amplitude and phase components. For further details, refer to the literature [26–28].

$$S = A \exp(-j\varphi) \quad (1)$$

where A and φ are the amplitude and phase, respectively, corresponding to one pixel. Figure 2 illustrates a spaceborne SAR image. The amplitude in Figure 2a indicates radar signal strength of the ground features and the phase in Figure 2b records the distance between the antenna and ground target. The phase information is particularly valuable for radar interferometry-based deformation monitoring techniques.

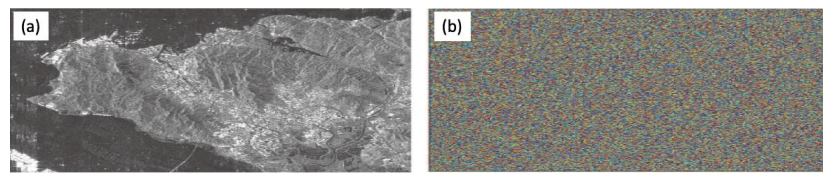


Figure 2. The amplitude (a) and phase (b) components of an SAR image covering part of Hong Kong.

Radar interferometry detects deformation by analyzing the range difference between two (or more) acquisitions to the same target, known as differential distance (ΔR), as shown in Figure 1. Generally, the differential phase can be achieved by complex conjugation of two SAR images (e.g., S_1 and S_2) to generate an interferogram (IFG) as shown in Equation (2) as follows:

$$IFG = S_1 S_2^* = A_1 A_2 \exp(-j(\varphi_1 - \varphi_2)) = A_{1,2} \exp(-j\Delta\varphi_{1,2}) \quad (2)$$

where $*$ indicates the complex conjugate operation. Ideally, by calculating the phase difference, $\Delta\varphi_{1,2}$, the deformation of the ground surface can be obtained by phase unwrapping of $\Delta\varphi_{1,2}$. However, in practical applications, it is not easy to achieve accurate deformation measurement in this way because the phase difference may be subject to various disturbances during the transmissions, such as atmospheric turbulence, surface reflection, signal multiple reflections, etc.

2.2. Development of Radar Interferometry Techniques

2.2.1. Spaceborne InSAR

As introduced in Section 2.1, radar interferometry measures distance changes between the ground target and the satellite. However, acquiring SAR images using a spaceborne SAR sensor at different times leads to varying positions of the satellite, as illustrated in Figure 3 [29–31]. This complicates precise deformation retrieval [32,33]. After the complex conjugate operation to achieve the phase difference, the interferometric phase mainly has five phase components [31].

$$\Delta\varphi_{1,2} = w\{\varphi_1 - \varphi_2\} = w\left\{\Delta\varphi_{1,2}^{flat} + \Delta\varphi_{1,2}^{topo} + \Delta\varphi_{1,2}^{defo} + \Delta\varphi_{1,2}^{APS} + \Delta\varphi_{1,2}^{noise}\right\} \quad (3)$$

where $w\{\cdot\}$ stands for the phase wrapping operation, which wraps the interferometric phase into $(-\pi, \pi]$; $\Delta\varphi_{1,2}^{flat}$ stands for the flat reference phase; $\Delta\varphi_{1,2}^{topo}$ is the topographic phase; $\Delta\varphi_{1,2}^{defo}$ is the ground deformation phase reflecting the displacement of the target between the two SAR acquisitions; $\Delta\varphi_{1,2}^{APS}$ is the atmospheric phase screen (APS) related to the atmospheric delays; and $\Delta\varphi_{1,2}^{noise}$ stands for the noise phase.

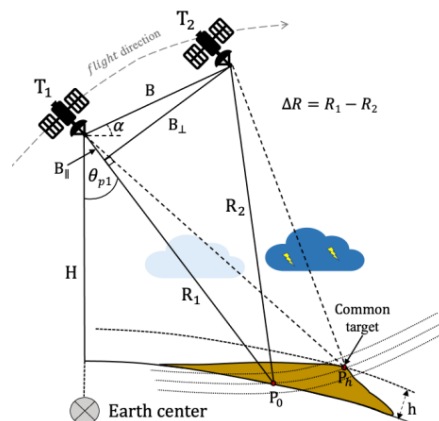


Figure 3. Schematic diagram of InSAR.

To retrieve the ground deformation, the unwanted signal in Equation (3) should be compensated as much as possible. The first two items can be compensated with satellite orbital information and a digital elevation model (DEM) [34]. Imperfections in orbital data and DEM may result in phase errors, as shown in Equation (4) [31,35].

$$\Delta\varphi_{1,2} = w \left\{ \Delta\varphi_{1,2}^{orb} + \frac{4\pi}{\lambda} \frac{B_{\perp}^{1,2}}{R \sin(\theta)} \Delta z^{error} + \frac{4\pi}{\lambda} \Delta d_{defo} + \Delta\varphi_{1,2}^{APS} + \Delta\varphi_{1,2}^{noise} \right\} \quad (4)$$

where R , θ , and λ are the distance between the satellite and the ground target, incidence angle, and radar wavelength; B_{\perp} is perpendicular baseline of the interferogram; and $\Delta\varphi_{1,2}^{orb}$ and Δz^{error} are the orbital error and DEM errors, respectively. In urban areas, the height of infrastructure is unrecorded in the used DEM products and often interpreted as the phase component related to the DEM error in an interferogram.

In Equation (4), the ground deformation can be retrieved through phase unwrapping when the deformation signal is the dominant interferometric phase, such as the deformation related to earthquakes [36,37]. For small-scale/subtle ground deformation, the deformation retrieval may be impaired by orbital error [38], DEM error [39], APS effect [40,41], and decorrelation noise [42]. Therefore, time series analysis of stacking IFGs, called multi-temporal InSAR (MT-InSAR), has been developed to minimize these effects since about the year 2000 [43]. In particular, two pioneering MT-InSAR frameworks have been proposed, namely Persistent Scatterers InSAR (PS-InSAR) [44,45] and Small Baseline Subset (SBAS) [46], which are the most popular techniques used to detect the temporal evolution of ground deformation.

The PS-InSAR framework employs a time series of SAR data to identify PS points with high phase stability for ground deformation detection. This framework does not take into account the impact of decorrelation caused by the length of the spatiotemporal baselines between SAR images [45]. On the other hand, the SBAS framework considers the decorrelation noise related to the baselines and suppresses the noise using points with higher phase quality from a subset of the IFGs with small spatiotemporal baselines [46]. The combination of PS-InSAR and SBAS have also been developed [47,48]. All these approaches aim to address the main challenges, such as the decorrelation noise, atmospheric delay effect, and the phase ambiguity issue.

One effective approach to minimize the decorrelation noise effect in the MT-InSAR framework is to focus solely on analyzing the pixels with high phase quality. This can be achieved through the application of various criteria, such as the amplitude dispersion index [45], spectral diversity [49], offset deviation [50], phase stability [51], coherence map [46], posterior coherence [48], and the integrated index [47]. It is important to highlight that the use of each criterion may lead to the identification of different ground targets, even when employing the same SAR dataset. The limitations associated with this issue are thoroughly discussed in Section 5.

To address the phase ambiguity issue, PS-InSAR first estimates the unwrapped double differential phase of point pairs, termed as arc, in the temporal domain, and then retrieves the unwrapped phase in the spatial domain in which the double differential phase is normally constructed by a spatial network by linking the selected point pairs, including the Delaunay network [45], the hierarchal network [52], and the constrained network [53]. A temporal deformation model is assumed to detrend the phase ramp on an arc of the network [54,55]. Multiple parameter estimators have been employed for retrieving the signal of interest, including periodogram analysis [45,55], integer least squares [54], and least squares with a phase ambiguity detector [56]. On the contrary, in the SBAS framework, the interferometric phase is first unwrapped in the spatial domain and then the unwrapped phase is integrated in the temporal domain. This strategy employs various spatial unwrapping methods, such as the path-tracking-based approach [36,57] that integrates the phase gradient field along optimized paths to obtain the unwrapped phase. Another type of

method is the global optimization-based approach [37,58], which minimizes the global difference between the unwrapped phase and the wrapped phase.

In addition to addressing these challenges, many new MT-InSAR methods or approaches also focus on precise parameter estimation or postprocessing [59,60]. For example, to enhance the quality of MT-InSAR results, much effort have been invested into modelling and mitigating, e.g., satellite orbital errors [61–64], atmospheric delays [65–69], ionospheric effects [70–73], DEM errors [59,74,75], co-registration errors [76–79], unwrapping errors [80–82], and errors in geocoding the measurements [83,84]. Several variations of MT-InSAR have been developed and implemented in software packages to address these problems and issues, including IPTA [49], STUN-PS [54], StaMPS [85], EMCF-SBAS [55], SqueeSAR [48], CPT [86], PSP [87], TCP-InSAR [56,88], CAESAR [89], CSI [90], LiCSAR [91], and D-TomoSAR [92]. Table 1 presents a brief overview of some of these MT-InSAR approaches and packages, while Figure 4 summarizes the SAR satellites that have provided SAR images.

Table 1. Examples of MT-InSAR methods/packages and their characteristics.

	MT-InSAR	Baseline Configuration	Observation Phase	Target Selection	Solver	Parameters
Methods	PS-InSAR [45]	Single-Master	Wrapped	ADI	Periodogram	$\Delta h, \Delta v$
	SBAS [46]	Multi-Master	Unwrapped	Coherence	Least squares	$h,$
	CPT [86]	Single/Multiple-Master	Wrapped	Signal-to-clutter ratio	Conjugate gradient method	$\Delta h, \Delta v$
	SqueeSAR [48]	Single-Master	Wrapped	Homogeneity test	Periodogram	$\Delta h, \Delta v$
	CEASAR [89]	Single/Multiple-Master	Wrapped	ADI/Homogeneity test	PCA/Periodogram	$\Delta h, \Delta v$
	TCP-InSAR [56,88]	Multi-Master	Wrapped	Offset deviation	Least squares	$\Delta h, \Delta v$
	D-TomoSAR [92]	Single-Master	Wrapped	ADI	Compressed sensing	$\Delta h, \Delta v$
Packages	STUN-PS [54]	Single-Master	Wrapped	ADI	Integer least squares	$\Delta h, \Delta v$
	StaMPS [85]	Single/Multiple-Master	Wrapped	Phase stability	3D phase unwrapping	-
	IPTA [49]	Single/Multiple-Master	Wrapped	ADI	Periodogram	$\Delta h, \Delta v$
	QPS-InSAR [93]	Target-dependent interferogram subset	Wrapped	Quasi-PS	Periodogram	$\Delta h, \Delta v$
	EMCF-SBAS [55]	Multi-Master	Wrapped	Coherence	Minimum cost flow	$\Delta h, \Delta v$
	PSP-IFISAR [87]	Single/Multiple-Master	Wrapped	ADI	Minimum cost flow	$\Delta h, \Delta v$
	CSI [90]	Single/Multiple-Master	Wrapped	Homogeneity test	Periodogram	$\Delta h, \Delta v$
	LiCSAR [91]	Single/Multiple-Master	Unwrapped	Coherence	-	-

ADI: amplitude dispersion index; PCA: principal component analysis.

2.2.2. GBRI Technique

GBRI works on a similar principle as spaceborne InSAR technology but utilizes a radar system located on the ground. As ground radar is superior in its portability, it can be flexibly configured in different locations according to specific needs, as shown in Figure 5. When the system is placed in a fixed position, it generally enables the acquisition of radar images with a zero baseline, and the first two phase terms in Equation (3), $\Delta\phi_{1,2}^{flat}$ and $\Delta\phi_{1,2}^{topo}$, will not exist. The interferometric phase therefore can be written as depicted in [94,95] as the following equation:

$$\Delta\phi_{1,2} = w\{\varphi_1 - \varphi_2\} = w\left\{\Delta\phi_{1,2}^{defo} + \Delta\phi_{1,2}^{APS} + \Delta\phi_{1,2}^{noise}\right\} \quad (5)$$

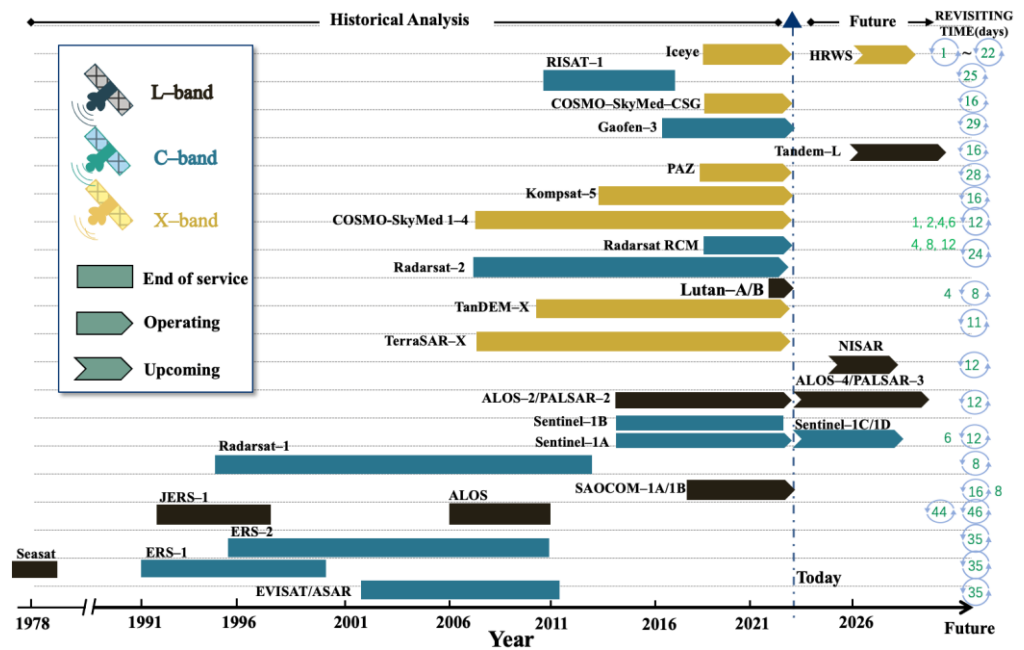


Figure 4. Past, currently operating, and upcoming SAR satellites.

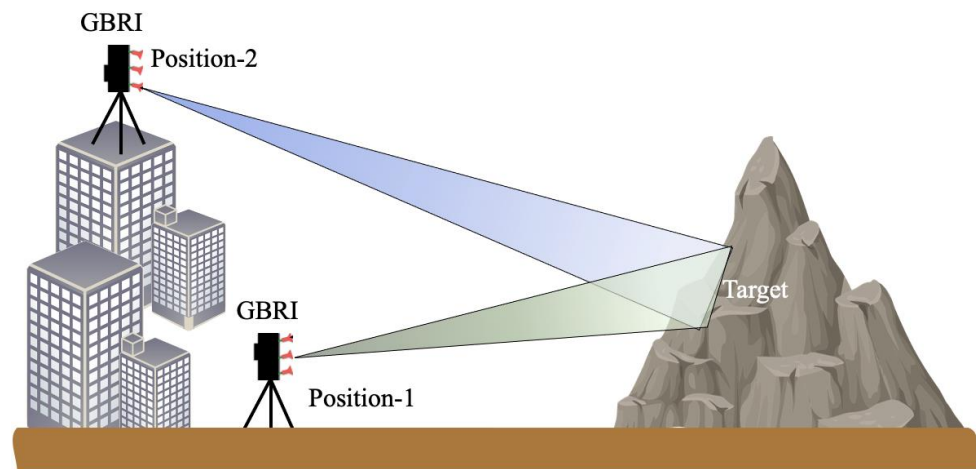


Figure 5. Observational geometry of the GBRI system in various configuration positions.

In Equation (5), deriving deformation from GBRI observations is still not a straightforward task. The accuracy of a GBRI remains susceptible to the decorrelation noise, the atmospheric delay, and the ambiguous nature of the interferometric phase. Numerous investigations have been conducted to alleviate the effects of decorrelation and APS on ground-based radar observations [96]. In particular, to mitigate the decorrelation effect, artificial corner reflectors and stable point analysis approaches are often employed [97,98]. To address the APS effect, various numerical models have been developed, such as the polynomial model [99,100]. In addition, techniques borrowed from spaceborne InSAR techniques, such as PS-InSAR, have also been implemented in GBRI applications to counteract the APS effect and decorrelation noise [101–104].

Although utilizing a fixed station for a ground-based radar can effectively mitigate the baseline errors, resetting up the instrument in the case of using a tripod may still result in baseline errors [105,106]. To address this issue, various studies have been conducted to model the errors in a solution [107,108]. It has demonstrated that the precision of a GBRI system can reach up to a sub-millimeter level when artificial targets are measured [109–112]. Due to the high precision and adjustable observational geometry of a GBRI system, it has been widely used in urban infrastructure stability monitoring, including both large-scale and individual-target monitoring [24].

Radar bands ranging from C-band to Ku-band have been used to enhance the sensitivity of ground-based radars to high-frequency deformation such as the vibration of bridges. Radar types have been updated from the Stepped Frequency Continuous Waveform (SFCW) to the Frequency Modulated Continuous Wave (FMCW) to minimize the duration of data collection [24,95]. Figure 6 gives some types of existing ground-based radar systems with diverse features [94,95]. Figure 6a shows the GPRI-II system equipped with a slotted waveguide antenna. This antenna enables the generation of radar datasets using both a real aperture imaging mode in the LOS direction and the SAR imaging mode through the rotation of the antenna in the azimuth direction. Figure 6b shows a synthetic aperture system with a horn-shaped antenna, whereas the real aperture antenna produces a relatively wider cone-shaped beam as shown in Figure 6e. A dish antenna is used in the radar system in Figure 6c that can produce a narrow pencil-shaped beam. Figure 6d shows the radar system that can improve the horizontal coverage (i.e., full 360°) of the measurements with a new design. Table 2 provides a concise overview of the commonly used GBRI systems and their distinctive features. Detailed technical specifications can be accessed in [94,95].

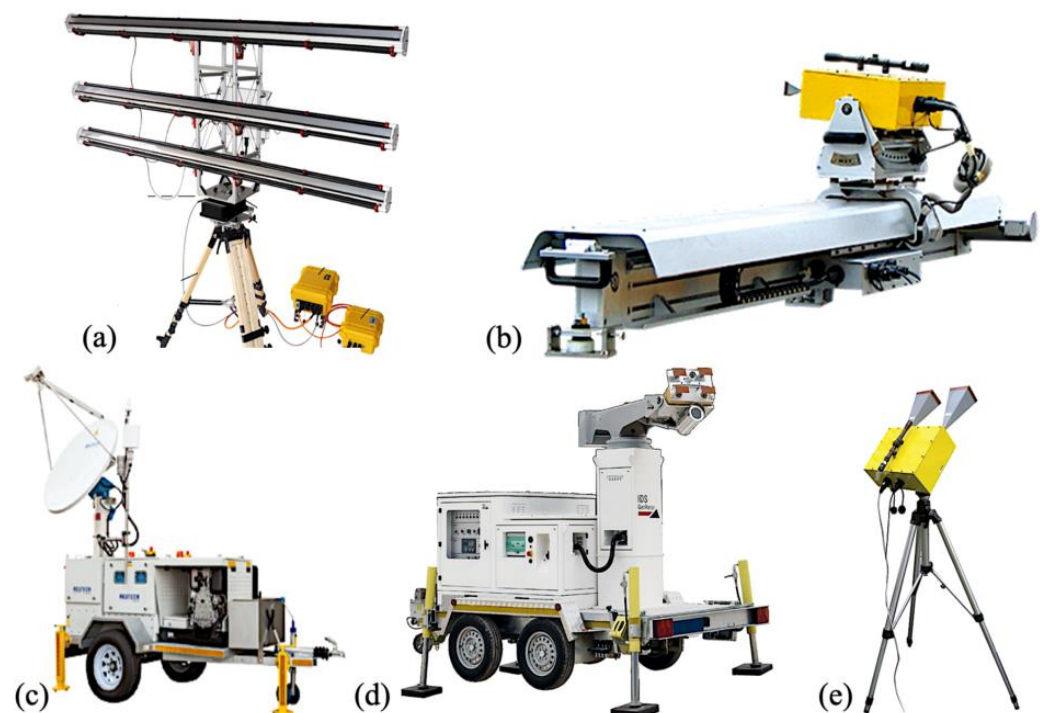


Figure 6. Examples of different ground-based radar systems. GPRI-II (a), IBIS-FM (b), MSR400 (c), IBIS-ArcSAR (d), and IBIS-FS (e).

Table 2. Summary of the commonly used GBRI systems.

Name	Lisa	RiskSAR	GPRI-II	IBIS-L/M	Melissa	SSR	FastGBSAR
Developer	JRC	Technical University of Catalonia	GAMMA remote sensing	IDS spa Tohoku University	JRC (EC)	GROUNDPROBE	MetaSensing (NL)
Radar type	VNA	FMCW	FMCW	SFCW	MIMO	Mechanical Scanning	FMCW
Antenna type	-	Pyramidal horn	Slotted waveguide	-	Horn/Vivaldi	Linear/Disc	-
Wavelength and polarization	C (VV, HH) Ku (VH, HV)	X (VV, HH)	Ku (VV, HH, VH, HV)	Ku (VV)	Ku (VV)	Ku (VV)	Ku (NA)
Measurement range	3 km	10 km	0.05–10 km	0.2–4 km	4 km	5.6 km	4 km
Range resolution	0.5 m	1.25 m	0.75 m	0.5/0.75 m	-	0.75 m	0.5/0.75 m
Azimuth resolution	3 m	4 m	6.8 m	4.4 m	-	9 m	4.5 m
Maximum sampling frequency	-	50 MHz	4000 Hz	-	25 MHz	-	4000 Hz
Radar image product	2D	2D	1D and 2D	2D	2D	2D and 3D	2D
Displacement accuracy	0.02–4 mm	1.6 mm	0.02–4 mm	0.03–4 mm	-	0.03–3.5 mm	0.1 mm

VNA: vector network analyzer; MIMO: multiple-input multiple-output.

2.3. Characteristics

This section will introduce the unique characteristics of radar interferometry.

2.3.1. LOS Observation

The radar antenna is usually mounted on a platform and measures deformation along the LOS direction. This generates an incident angle between the LOS direction and the normal line of the ground surface, determining the observation geometry of the radar. For convenience, we will introduce it to a spaceborne InSAR. Figure 7a illustrates the geometry of the spaceborne SAR system for observing deformation. The detectable deformation along the LOS relies on both the direction of the actual deformation and the radar observational geometry. The incident angle (θ) and heading angle (β) determine the portion of the deformation projected onto the LOS direction, which can be expressed as [113] the following equation.

$$D_{los} = D_n \sin \theta \sin \beta - D_e \sin \theta \cos \beta + D_u \cos \theta \quad (6)$$

where D_u , D_n , and D_e are the elements of the deformation vector along the up–down, north–south, and east–west directions, respectively. The near-polar orbits of the current SAR satellites lead to either the ascending ($\beta \approx -12^\circ$) or descending ($\beta \approx 191^\circ$) of orbital geometry. The top view of the geometry is illustrated in Figure 7b,c. According to Equation (6), Figure 8 demonstrates the sensitivity of the LOS deformation for these two geometries to the incident angles. The contributions of the deformation in the eastern direction to the radar LOS direction are opposite in the ascending and descending orbits. This problem will be discussed in Section 5.

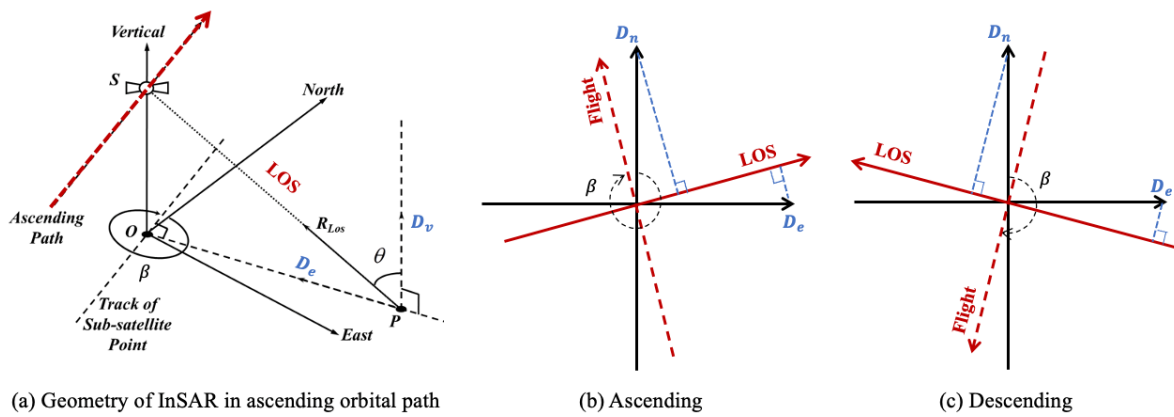


Figure 7. Observational geometry of the spaceborne radar system.

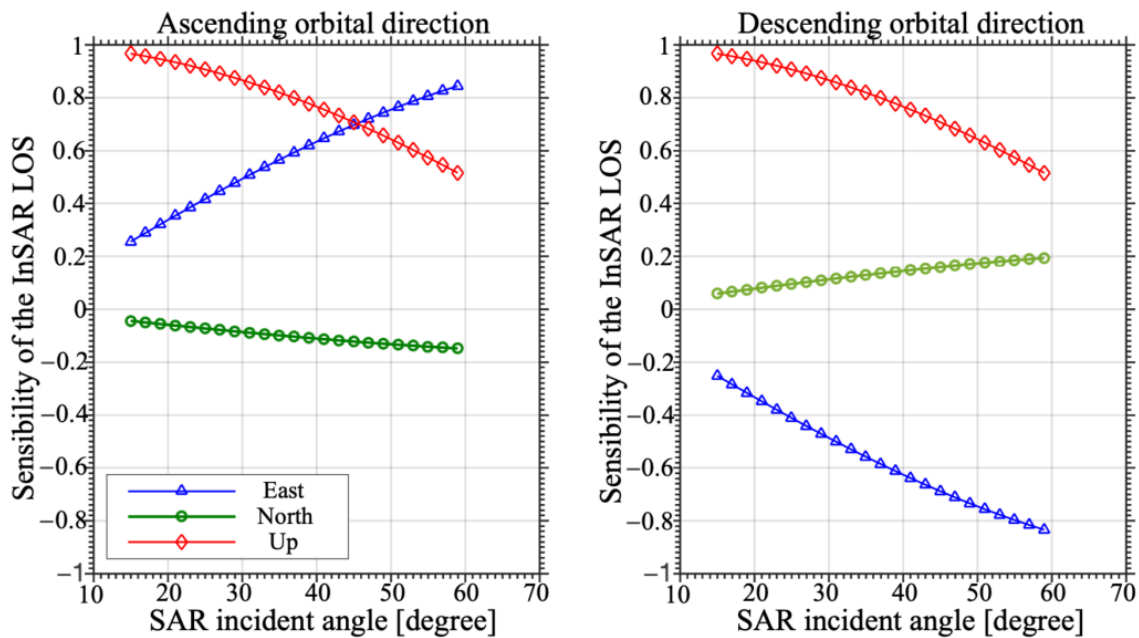


Figure 8. Sensibility of the radar LOS deformation to the SAR incident angles [114].

2.3.2. Geometrical Distortions

Geometrical distortion is another unique characteristic of spaceborne InSAR that can cause errors in the measured deformation due to the LOS observational geometry [31]. Figure 9 illustrates geometric distortions in SAR images due to the radar’s ranging nature and the interplay between terrain slope and angle of incidence. Distortions include foreshortening, layover, and shadows. The perspective foreshortening happens when the local inclination angle facing the SAR sensor and the terrain slope angle is smaller than the local incidence angle, resulting in a shorter slope length in an SAR image than in flat terrain [115]. When the local terrain slope angle equals the local incidence angle, the slope is recorded as one pixel in the SAR image. If the local terrain slope angle surpasses the local incidence angle, cascading effects can occur, causing inverted images at the top and bottom of a slope. The radar sensor cannot receive signals from a steep slope beyond the local incident angle, resulting in a shadow effect that makes the slope appear darker in the SAR image. It is worth noting that geometrical distortion is more severe in urban areas due to the variation in the heights of the infrastructures, which will be discussed further in Section 5.

InSAR processing was used to detect ground deformation in various applications and assess the potential risks of urban infrastructures caused by the deformation (Figure 10b) due to groundwater withdrawal [137], soil consolidation [132], tunnel construction [138], land reclamation and underground construction [139], and slope instability [140].

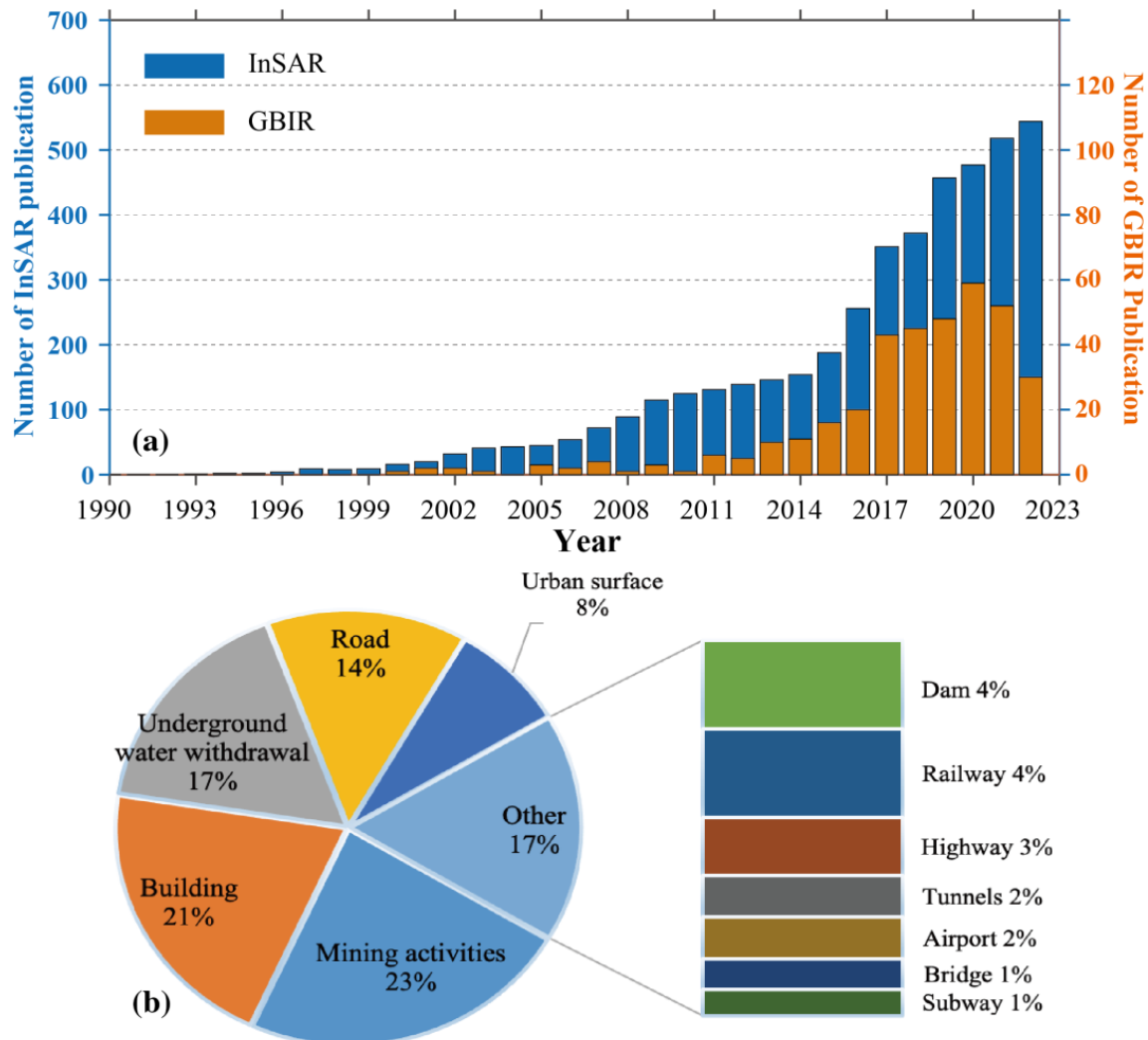


Figure 10. Annual number of journal papers on radar interferometric techniques and monitoring of urban infrastructures (a) and types of the infrastructures (b).

In recent decades, the rapid development and widespread availability of SAR data have significantly contributed to the advancements in radar interferometric techniques for monitoring the stability conditions of urban infrastructures. As shown in Figure 4, the increased availability of SAR data from various satellites, such as TerreSAR-X and COSMO-SkyMed, with high spatial resolution up to about one meter [141,142], has propelled the InSAR technique into its third stage of development. This stage has enabled researchers to investigate the deformation and stability of urban infrastructures of various sizes, including a wide range of buildings [143], and constructions such as bridges [144], railways [145,146], road networks [147], and dams [11,148]. The significant increase in the number of publications related to the monitoring of the stability conditions of urban infrastructures since 2007 is illustrated in Figure 10a. The launch of the Sentinel-1A/B (S1A/B) constellation in 2014/2016 marked the beginning of the fourth stage of InSAR technique development. This stage has witnessed significant advancements in the monitoring of urban infrastructures using InSAR, thanks to the cost-effectiveness and near real-time capabilities offered by the Sentinel-1 satellites. With short revisit time intervals of six days (despite the failure of the

S1B, which will soon be replaced by S1C) and free accessibility [149], the Sentinel-1 constellation has revolutionized the field of urban infrastructure monitoring. The use of InSAR for monitoring urban infrastructures has grown beyond local and regional coverages, enabling researchers to monitor urban infrastructures on a national scale [150,151]. The literature in Figure 10a clearly reflects the accelerated pace of research in the field of monitoring urban infrastructures since 2015.

Ground-based radar interferometry known as GBRI has emerged as a valuable and increasingly utilized technique for monitoring urban infrastructure deformation in recent decades [152]. The pioneering introduction of the outdoor portable SAR system called LISA (Linear SAR) in 1997 marked the inception of possibilities for studying concrete girder deformation [22]. As illustrated in Figure 10a, initially, few GBRI applications have been conducted for urban infrastructure monitoring, primarily finding use in various geohazard-related applications such as monitoring landslides [21], glaciers [153], and open-pit mining [154]. For further details, refer to [24,155]. However, over the recent decade, the use of GBSAR-based techniques has significantly grown, mainly due to their unique characteristics, notably portability and high spatial, and temporal sampling capabilities [156].

In the context of urban infrastructure monitoring, GBRI has demonstrated remarkable performance in monitoring the stability of civil infrastructures such as man-made slopes [157] and dams [158]. Its high spatial and temporal sampling capability further enhances its effectiveness in monitoring the stability of the infrastructures, including high-rise buildings and bridges [159–161]. Recent studies have carried out the application using the GBSAR in monitoring high-frequency structural vibrations [162] and assessing the stability of underground tunnels and pipelines during construction activities [163]. Additionally, GBSAR has been used as a supplement to existing deformation monitoring techniques, strengthening its application for urban infrastructure monitoring [164]. To ensure precise interpretation of GBSAR results, accurate geocoding techniques have been employed, utilizing external DEM products [165] and terrestrial laser scanners [166]. Furthermore, the integration of GBSAR with other advanced technologies, such as GPS measurements [167] and artificial intelligence [168], has extended its capabilities during the deformation monitoring.

4. Recent Advances and Applications

This section will introduce the major advances and applications of the spaceborne InSAR- and GBRI-based techniques over the recent decade for monitoring stability conditions of urban infrastructures.

4.1. Monitoring of Multi-Dimensional Deformation of Infrastructure

The main objective of radar interferometry technology, when used for urban infrastructure monitoring, is to detect actual deformation of the infrastructures and identify potential risks from anomalous deformation. In ground subsidence monitoring related to, e.g., groundwater withdrawal and soil consolidation, the focus has been to convert the LOS deformation measurements to the vertical direction (see Section 3) [169]. In the recent decade, many studies have shown that it is not enough to accurately capture the motion of infrastructure in the LOS direction in practical applications. Urban infrastructure may experience both vertical and horizontal deformation, which cannot be reflected in a single LOS direction (see Section 2.3.1). Figure 11 gives an example of the deformation of a subway station under construction in Hong Kong, which has been verified to suffer both vertical and horizontal deformations [170]. Two SAR datasets, one from the ascending orbit direction and one from the descending orbit direction, were utilized to detect the LOS deformations (Figure 11a,b). The deforming locations were identified on the opposite sides of the street by different datasets due to the different sensitivities of the deformation to the LOS direction, as shown in Figure 11.

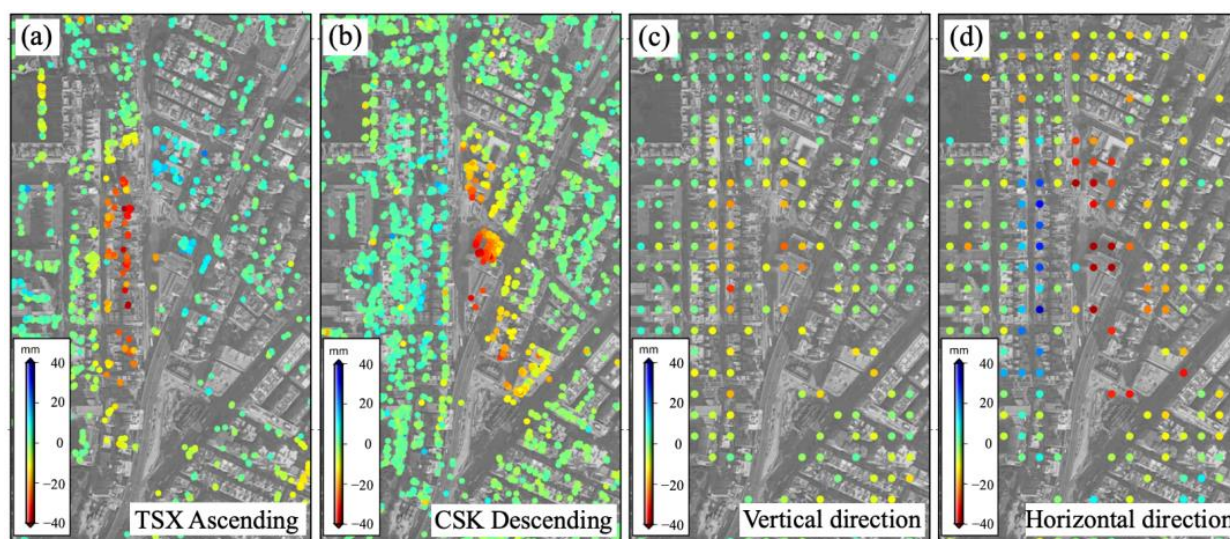


Figure 11. Deformation maps obtained using ascending TerraSAR–X dataset (a) and descending COSMO–SkyMed dataset (b). The decomposed deformation in vertical (c) and horizontal (d) directions. Background image is a Google Map image.

To obtain a more accurate representation of true deformation, joint analysis of SAR images from different orbital geometries has been carried out in recent decades by applying formulations of Equation (6) to decompose the LOS deformation estimates into two dimensions, i.e., the horizontal (east and west) and vertical directions (up and down) [114,171]. Figure 11c,d show the deformation rate by spaceborne InSAR over the subway station after decomposing the LOS deformation into the vertical and horizontal directions, indicating that this station suffered deformation in both directions. A GBRI system benefits from its portability and flexibility to adjust to an optimal observation geometry. The LOS observations are generally less affected by geometric issues during an application. For example, positioning a GBRI with the LOS parallel to the direction of the displacement provides the most favorable configuration. However, when the LOS is inevitably set at an angle in the direction of the displacement, the LOS deformation does not reflect the true deformation. To solve this problem, joint analysis of data from multiple ground-based radar systems have been conducted in many applications to achieve more realistic 2D [172] and 3D [173–175] deformations of urban infrastructures.

4.2. Detection of Anomalous Deformation of Infrastructures

When evaluating the stability conditions of urban infrastructures, engineers may be more interested in the anomalous deformation that poses a risk to structural safety. Radar interferometry techniques can detect any deformation that causes distance change along the LOS direction (see Section 2.1), including the normal behaviors of an infrastructure such as structural vibrations, thermal dilation [176,177], concrete shrinkage [178], and various errors. It is important to separate the errors from the deformation, and (often) also the anomalous structural deformation from the normal structural deformation. Advanced methods and models have been developed for this purpose. For example, APS compensation [179] and reference point correction [12] have been developed to mitigate the errors. Some studies have combined the finite element model [180], engineering knowledge [10], and radar deformation results for a joint analysis to detect the anomalous deformation [181]. Figure 12 illustrates the deformation rate (Figure 12a) and deformation time series (Figure 12b) observed over a subway line construction area in Shenzhen, China. To isolate the effects of thermal dilation on the infrastructure, the deformation attributed to this factor has been removed. Figure 12c highlights the specific period of anomalous deformation that occurred during the underground construction activities.

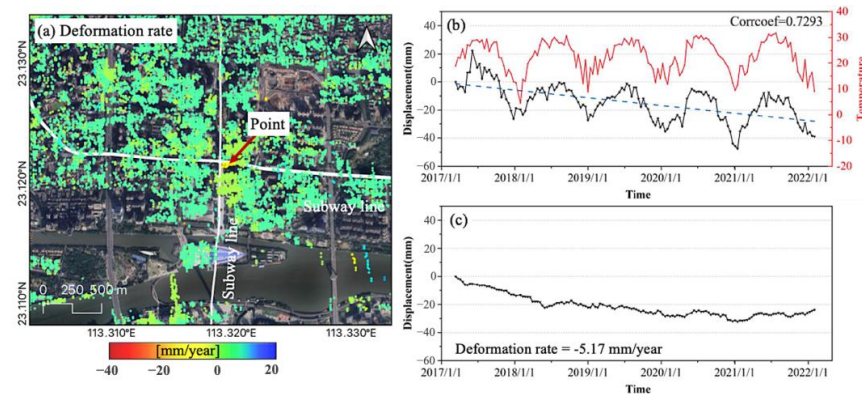


Figure 12. (a) Ground deformation rate map. (b) Observed deformation time series at selected points (black) and the temperature time series (red). (c) Anomalous deformation after separation of the deformation related to the thermal dilation. Background image is a Google Map image.

4.3. Accurate 3D Geolocation of Radar Measurements

Accurate geolocation of radar measurements in a three-dimensional (3D) reference frame is crucial in engineering, especially in the maintenance operations where precise identification of deformation locations is necessary. However, in radar interferometry, the interferometric phase not only records the deformation but also includes the DEM errors (Equation (4)). Such errors can have an impact on the accuracy of both the deformation measurements and the 3D geographic coordinates, particularly in urban infrastructure monitoring, where the infrastructures can introduce significant DEM errors. Therefore, the accuracy of the height estimation is crucial in radar interferometry to ensure precise 3D measurement positioning and accurate deformation interpretation in urban infrastructure monitoring [182]. Figure 13a–d shows how the variation in building height estimation can result in different levels of positioning accuracy when matched with the 3D model of Google Earth. To address these issues, several studies have developed advanced methods to enhance the accuracy of DEM error estimation and geolocation refinement [74,83,183]. By estimating the precise DEM error for calculating the geographic coordinates, even if two different SAR datasets are used, the geographical distribution of radar measurements from two datasets can still be consistent, as displayed in Figure 14. Furthermore, the Tomographic SAR (TomoSAR) technique has been utilized to retrieve point clouds for 4D urban models, whereas the 3D stands for the urban model, and 1D for the deformation [184–187]. In GBRI, terrestrial laser scanners and DEM generated through GBRI have been used to enhance the accuracy of geolocation [97,188–190].

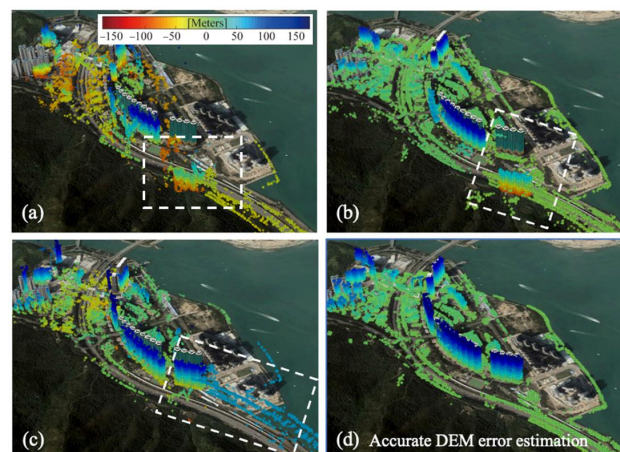


Figure 13. Reconstructed geolocation of InSAR measurements using estimated building height with different accuracies. The white box in (a–c) indicate the significant error in geolocation.

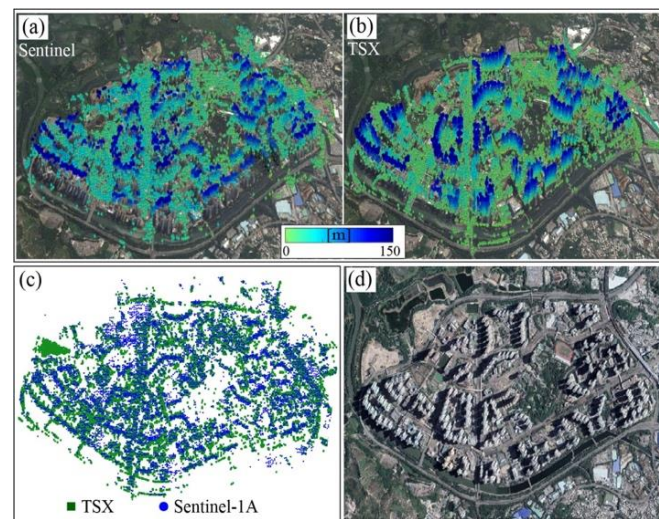


Figure 14. Estimated building height with Sentinel-1A (a) and TSX SAR datasets (b). (c) Top view of the distribution map of the coherent points. (d) Google image of the studied area.

4.4. Utilization of Multi-Platform Radar Interferometric Datasets

Over the recent decade, several studies have combined multiple datasets of SAR images to analyze long-term (e.g., decades) ground deformation in urban areas [191–193]. These studies have also carried out the thematic classification of urban hazards [194,195]. By employing multi-platform spaceborne SAR datasets, they have showcased the potential of long-term monitoring for mapping ground deformation and hazards in urban areas. For example, Figure 15 illustrates the ground deformation associated with the land reclamation, which was observed at Hong Kong International Airport (HKIA) through the employment of Envisat ASAR, CSK, and Sentinel-1A SAR datasets. The points density varies according to the spatial resolution of the SAR datasets employed. Following the resampling of deformation data, Figure 15d presents the cumulative ground deformation observed over decades [170]. It can be seen that the application of different SAR datasets to monitor ground deformation has different characteristics. A more detailed comparison discussion on the impact of SAR datasets with different spatial resolutions and wavelengths on deformation extraction can be found in [196–198]. Furthermore, studies have also been conducted to join the analysis of spaceborne InSAR and GBRI datasets to fully explore infrastructural damage [199].

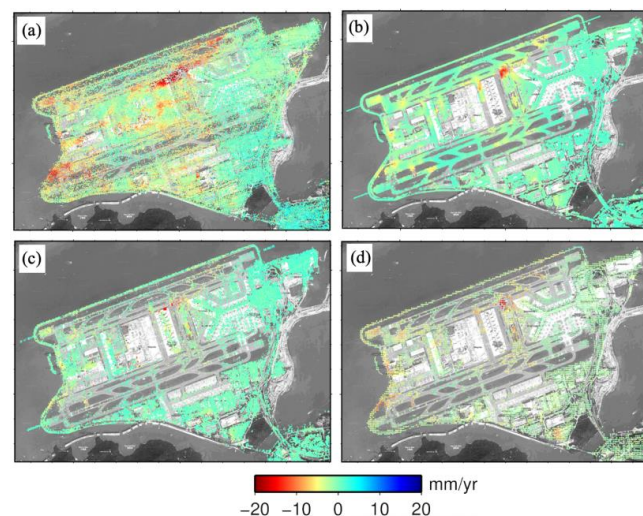


Figure 15. Estimated LOS ground deformation rate of the HKIA with (a) ASAR, (b) CSK, and (c) Sentinel-1A SAR datasets [170]. (d) Long-term ground deformation over the common points.

4.5. General Survey of Urban Surface Deformation

The radar interferometry technique has proven to be valuable for conducting general surveys of urban surface deformation. Its ability to cover large ground areas allows for comprehensive monitoring and analysis of ground movements. An example of such a survey took place in Nantong, China, where a Sentinel-1A dataset from 2015 to 2020 was utilized. This analysis unveiled significant deformations in the city, primarily attributed to groundwater withdrawal and the construction of a high-speed rail (refer to Figure 16). Additionally, this technology is useful for tracking ground deformation during urban construction projects. Figure 17 provides an illustration of the deformations caused by underground tunnel construction using high-resolution data from CSK satellites. In recent times, spaceborne InSAR has advanced to cover even larger scales. A famous example is the European Ground Motion Service (EGMS), which can provide a general survey of the ground deformation across national borders with millimeter accuracy [200].

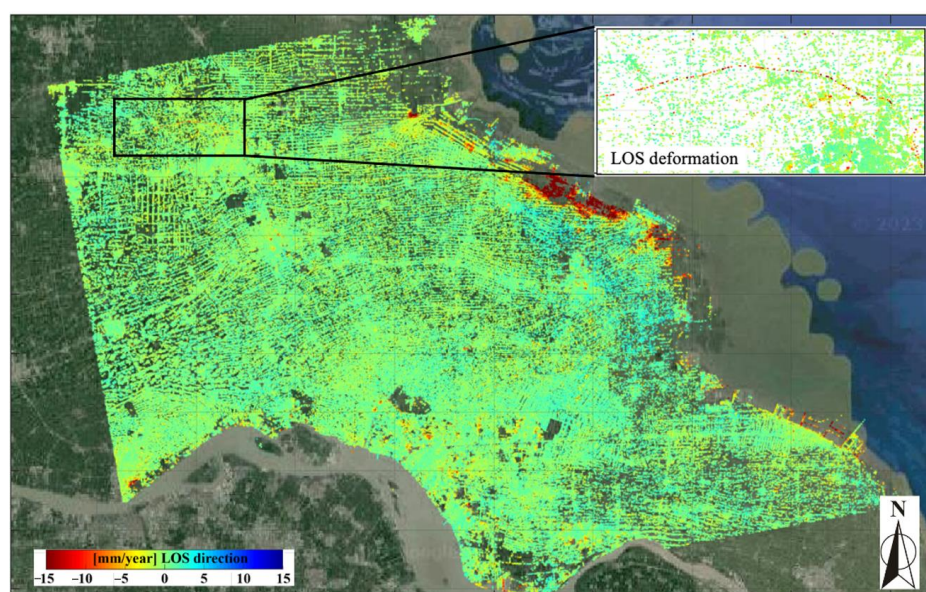


Figure 16. Estimated ground deformation rate with Sentinel-1A dataset in LOS direction over Nantong, China. Background image is a Google Map Image.

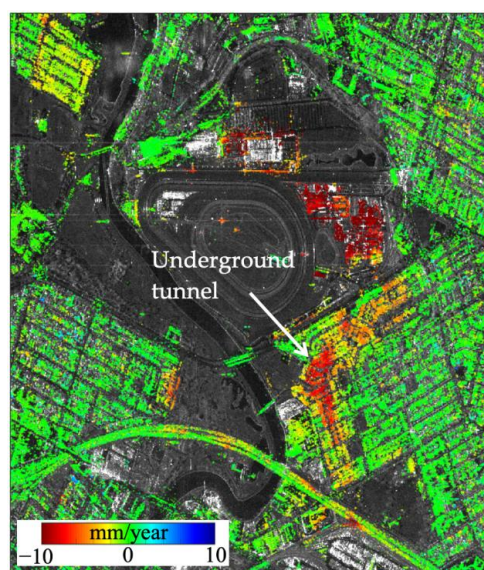


Figure 17. Estimated ground deformation rate with CSK dataset in LOS direction relating to the underground construction.

4.6. Fine Surveillance of Infrastructure Stability

Radar interferometry has become increasingly effective in monitoring the deformation of buildings and structures with fine resolutions. A number of studies have resulted in fine results showing the stability of infrastructures, including building cavity migration [201], deformation of dam structures [202,203], and stability of bridges [204]. Figure 18 demonstrates an example the use of InSAR and CSK data to detect fine building deformation signals overlaid on a Google Earth map. Figure 18b,c indicate thermal expansion and deformation anomalies of the buildings, respectively. It shows the ability of the spaceborne InSAR to precisely detect cumulative deformation, such as the thermal dilation that is greater at the top of a building than at the bottom [88]. Although the capability of spaceborne InSAR can be affected by geometric distortion, particularly in urban environments (see Section 2.3.2), the GBRI has been used as a complementary technique for individual structure deformation monitoring, allowing the capture of fine details and high-frequency deformations [167]. Figure 19 presents an application with the GPRI-II system for monitoring the high-frequency deformation of bridges using the real aperture imaging mode [159]. Figure 19a shows the natural vibration of the bridge, while Figure 19b,c depict the deformation caused by the crossing of one and two subway trains, respectively.

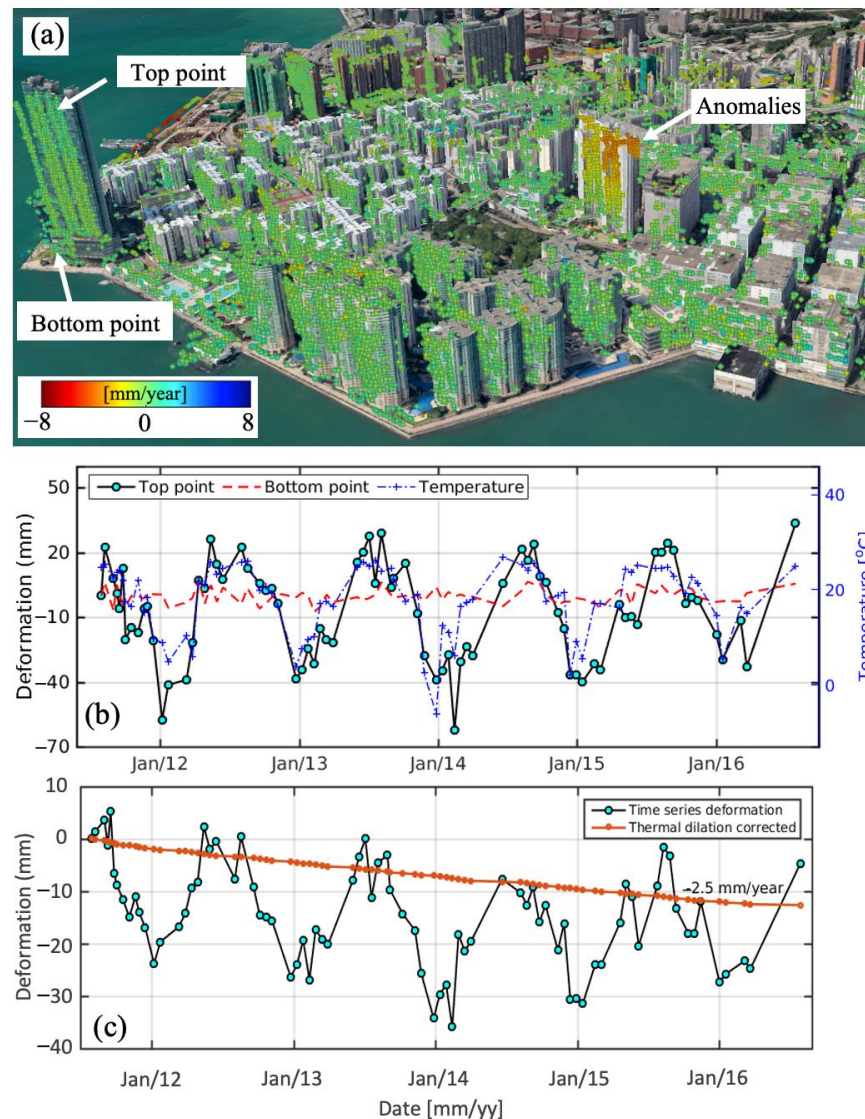


Figure 18. (a) Estimated LOS deformation rate of buildings with CSK dataset. (b) Thermal dilation of the buildings. (c) Building deformation time series after compensating the thermal dilation [88].

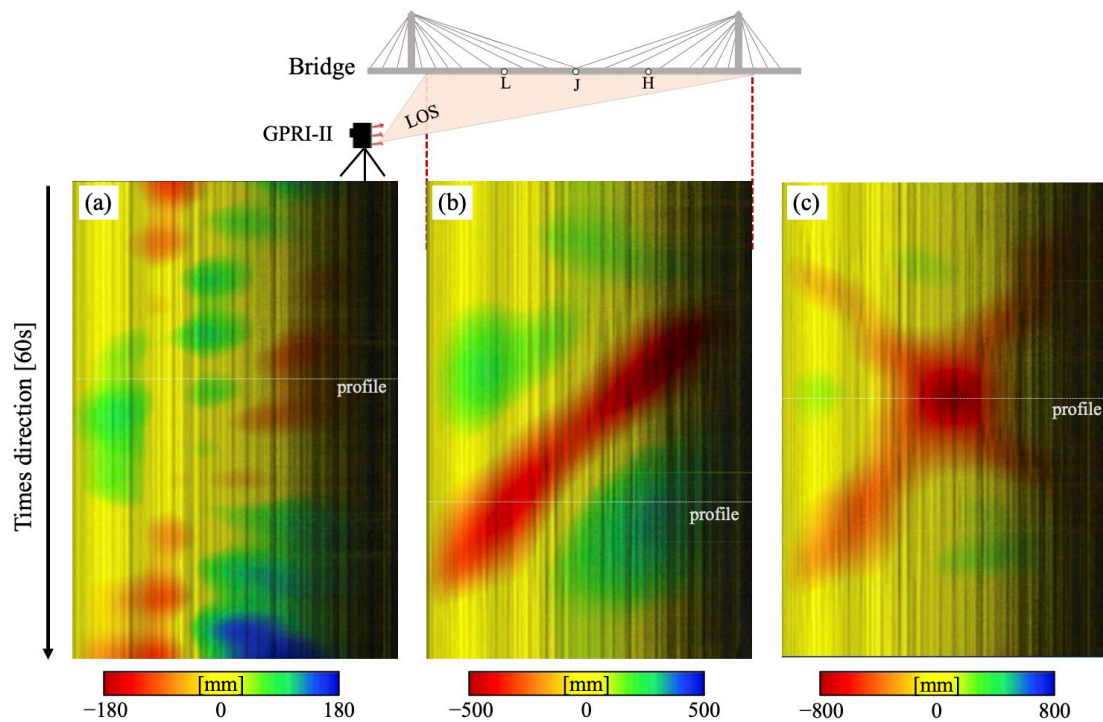


Figure 19. LOS deformation of a bridge in Hong Kong observed with a GPRI-II system [159]. (a) Bridge vibration without train crossing the bridge. (b) Bridge vibration when one train was crossing. (c) Bridge vibration when two trains were traveling opposite each other.

5. Challenges and Future Work

In this discussion, we will explore the challenges that may impede the effective use of spaceborne InSAR and GBRI for monitoring the stability of urban infrastructures. We will also outline some potential research questions that require further investigation.

5.1. Challenges

5.1.1. Inconsistent Spatial Distributions of Selected Measurements

As introduced in Section 2.2, selecting observable points with high phase quality in time series radar interferometric data processing is crucial to minimize decorrelation noise when determining deformation. Despite several proposed criteria for identifying such points, finding the most appropriate selection method remains a significant challenge, often relying on the operator's experience [205]. The impact of different selection criteria in spaceborne InSAR is evident in Figure 20, where varying results are observed. Furthermore, a steady stream of research proposing innovative point selection methods has demonstrated the existence of this phenomenon [206–208]. These research outcomes can be taken as an emphasis on the need for standardized and robust criteria to ensure consistent and reliable measurements in radar interferometric analysis.

In addition, the geometry of radar observation can also affect the observable points, particularly in urban areas where the infrastructures can have very different heights and orientations, affecting the distributions of the observable points. As a result, obtaining enough measurable points to monitor the deformation of specific infrastructures at the desired locations will be problematic. This is especially true when monitoring the highway distributed along the LOS direction, as shown in Figure 21; the targets of interest may not have enough measurable points, leading to an incomplete deformation map. On the other hand, the shadowing effect (see Section 2.3.2), which is more severe in dense urban areas such as Hong Kong, is another factor that affects the completeness of the distribution of radar measurements. Despite the ability to easily change the observation station, similar challenges can also arise when using a GBRI system. Therefore, careful consideration must

be given to these challenges and limitations when using radar interferometry for measuring deformation, particularly in the context of monitoring infrastructures with linear features.

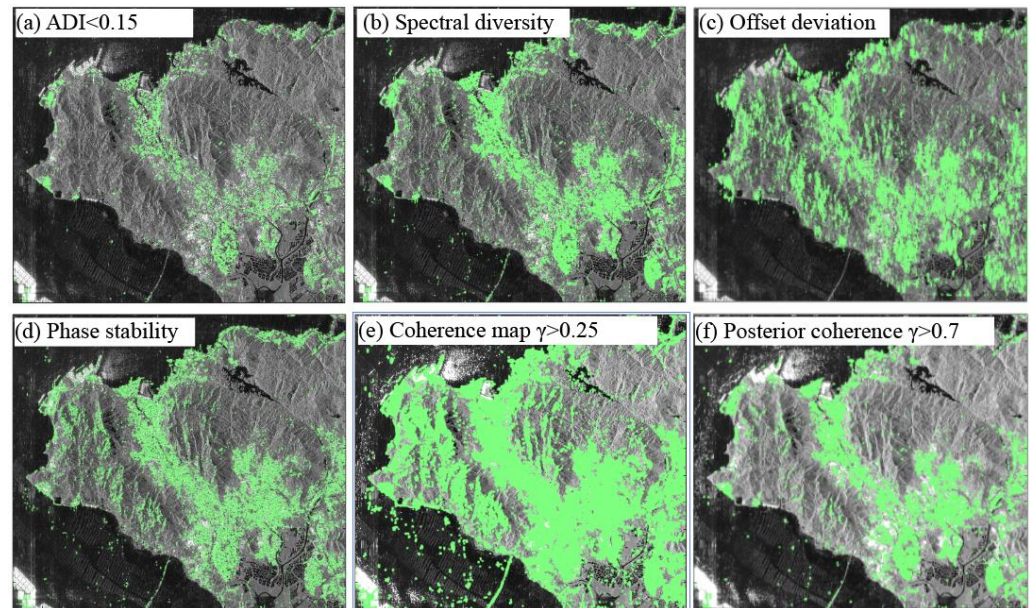


Figure 20. Coherent point identification with different criteria over the same area and the same SAR dataset.

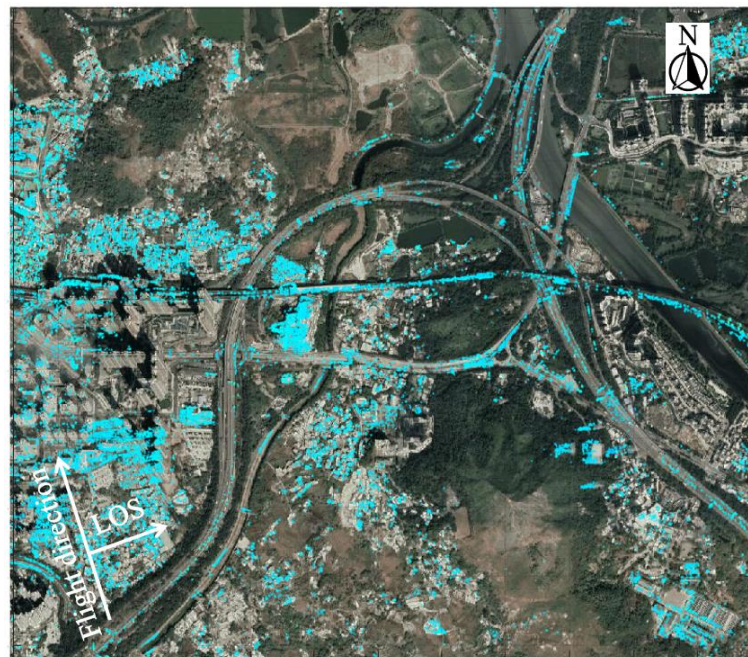


Figure 21. Example of point detection with InSAR. The background image is a Google Map image.

5.1.2. Difficulties in Phase Unwrapping

Phase unwrapping is one of the key steps in radar interferometric data processing, and its accuracy determines the accuracy of the final deformation results. As mentioned in Section 2.2, phase unwrapping is used to transform the wrapped phase into a continuous phase map. However, the complex urban surface features can generate a discontinuous phase, which reduces the accuracy of phase unwrapping [82]. Although studies have proposed some methods for advanced phase unwrapping and for unwrapping error cor-

rection [81,82,209,210], further work is still needed to improve the stability and accuracy of phase unwrapping in urban areas.

5.1.3. Areas of Rapid Urbanization

Urbanization can give rise to swift surface changes in urban regions, leading to rapid decorrelation and significant deformation gradients. Although GBRI proves effective for real-time deformation monitoring, achieving sufficient radar observations in certain urban areas remains a challenge. This is particularly evident in reclaimed areas where deformation and ground surface exhibit high variability. An illustration of this issue is provided in Figure 22, showcasing the deformation measurement results in a rapidly decorrelating land reclamation area in Macau, where both GBRI and spaceborne InSAR were utilized. Despite the use of GBRI, numerous regions appear blank and unobservable (refer to Figure 22a), which leads to the generation of incomplete deformation maps. To address these challenges, researchers have made effort on the aspects such as the distribution scatterer exploration [48,211–213], multi-satellite InSAR approach [214], and integration of radar interferometry with optical remote sensing [215] to retrieve the deformation over the rapid decorrelation areas in urban.

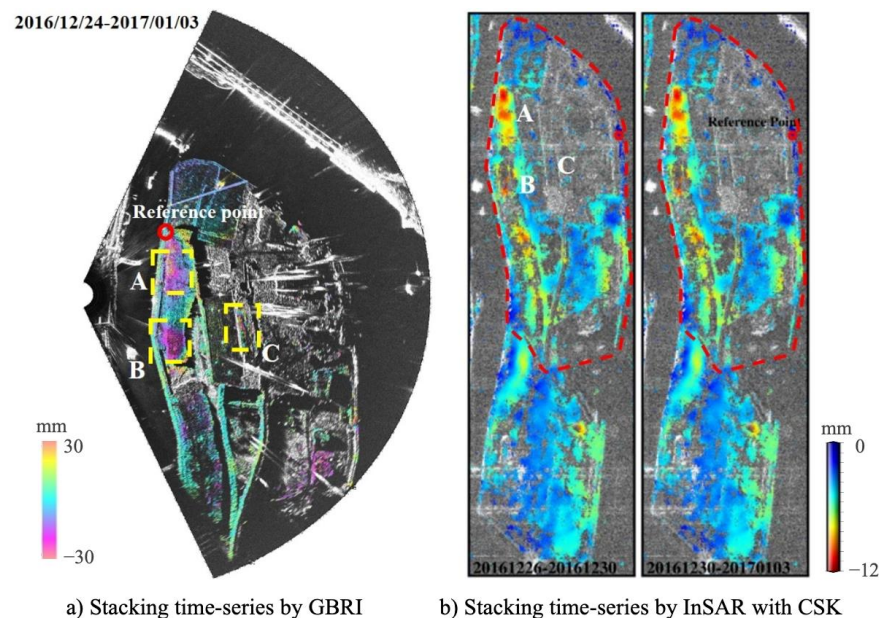


Figure 22. Deformation rate maps of a land reclamation area in Macau observed with (a) GBRI and (b) spaceborne InSAR. A, B, and C indicate the deformation area. The dot red line in (b) indicates a similar region to (a).

5.1.4. Geometric Distortions Caused by Urban Canyons

Geometry distortions, as introduced in Section 2.3.2, pose a significant challenge to radar interferometry in monitoring the stability conditions of urban infrastructures. This is particularly true in cities such as Hong Kong where dense tall buildings can easily create shadows in the radar images. Figure 23 gives an example of spaceborne InSAR measurements from a TSX ascending dataset covering a part of the Kowloon Peninsula in Hong Kong, as superimposed on a Google Earth map. Figure 23b shows a zoomed-in image where several ground areas and lower buildings are unobservable due to the obstructions of some tall buildings. As explained in Section 2.3.1, it is possible to obtain more information in such areas by combining ascending and descending SAR images. Thus, Figure 23c–e provide top-view maps of InSAR measurements for this region obtained from both ascending (TSX data) and descending orbits (CSK data). It is worth noting that some measurements of both sides of the buildings were obtained, but the roads between the buildings still remain unobservable. Therefore, it is crucial to have a clear understanding of

the targets being observed during the process of urban infrastructure stability monitoring. Focusing only on tall buildings could lead to misleading information, especially if the targets are the roads crossing the denser building regions.

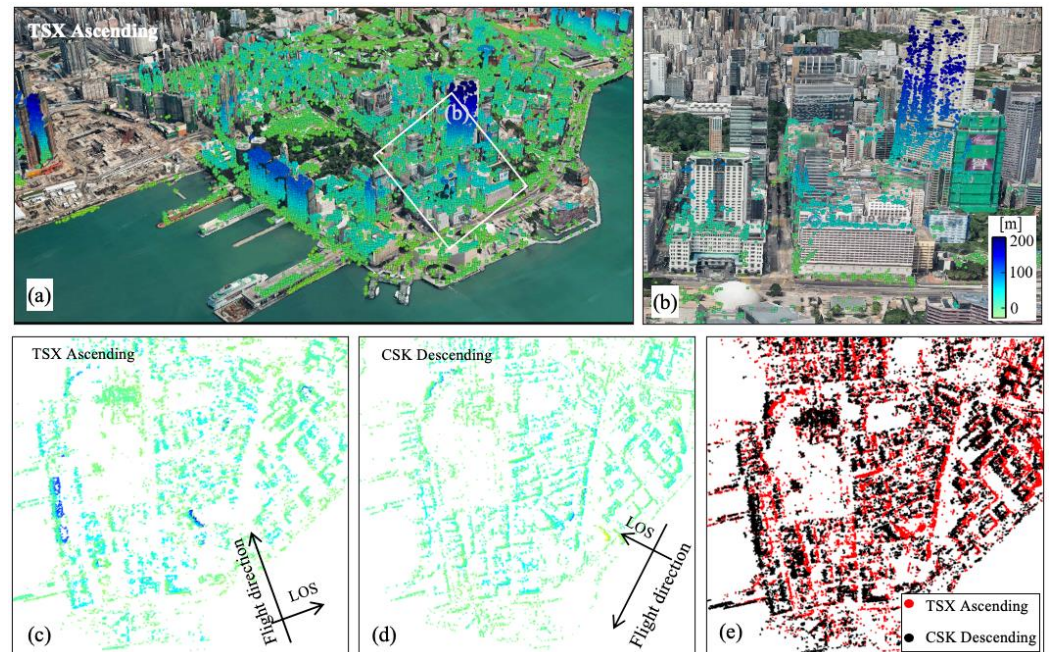


Figure 23. (a) The InSAR observable points of ascending TSX dataset overlaid on the Google Earth map. (b) Enlarged figure with different viewing angle. Parts (c–e) are top-view distributions of observable points in the ascending TSX and a descending CSK.

5.1.5. Appropriate Technology Selection for Structural Deformation Monitoring

Spaceborne InSAR and GBRI are valuable tools for monitoring various infrastructures. While spaceborne InSAR is effective for stable targets and offers wide coverage for large-scale structures, its long revisiting time limits its ability to capture rapid and dynamic movements. On the other hand, GBRI, specifically using the RAR mode, provides near real-time monitoring and detects dynamic behaviors with higher temporal resolution compared to spaceborne InSAR, which is generally used to monitor stable targets such as bridge piers and towers. It is particularly useful for monitoring structures with highly frequent motion, such as bridges under traffic loads or moving trains [162,216]. In the provided example of the Tsing Ma Bridge in Hong Kong (Figure 24), Figure 24b shows the deformation rate map obtained using spaceborne InSAR with a TSX dataset. It indicates a line-of-sight deformation rate of -30 mm/year in the central section of the bridge. However, interpreting this measurement directly may lead to a misunderstanding of the stability status of the bridge. In contrast, Figure 24c demonstrates the dynamic movements of the bridge captured with GBRI-II and GPS systems. It reveals displacements of over 40 cm and 70 cm in the vertical direction when one or two trains passed through the bridge, respectively. Figure 25 depicts the LOS deformation dynamics of tall buildings in Hong Kong, detected with the GPRI-II system using the RAR mode. The time series of deformation clearly demonstrates that GBRI offers distinct advantages in capturing highly dynamic deformations of infrastructures, enabling easy acquisition of structural vibration deformations at various frequencies. Consequently, it becomes paramount to thoroughly assess the strengths and weaknesses of each technology while conducting infrastructure security monitoring in order to monitor the corresponding characteristic deformations accurately.

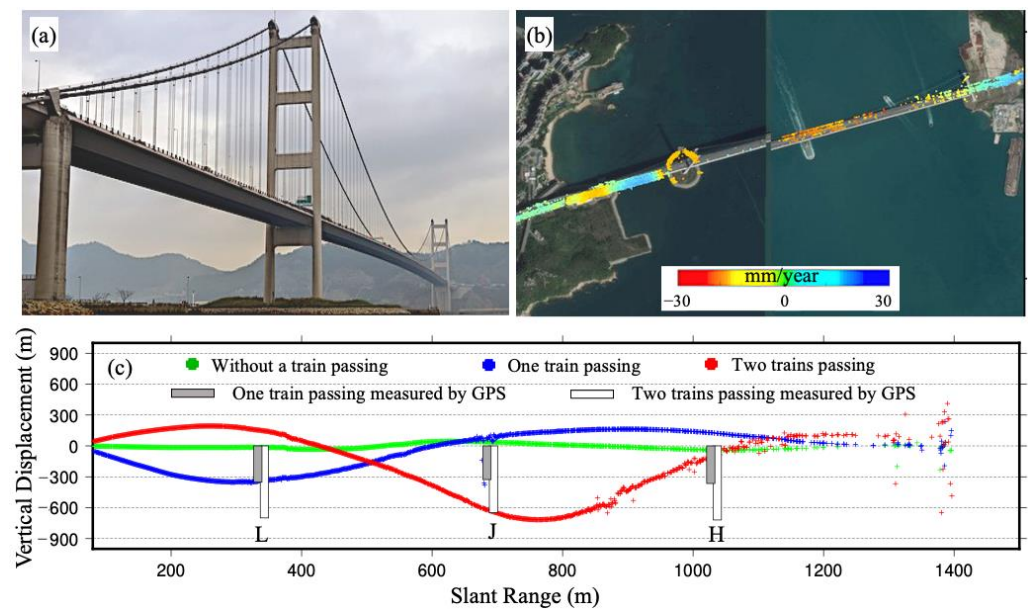


Figure 24. (a) Tsing Ma Bridge in Hong Kong. (b) The deformation rate of the bridge determined with spaceborne InSAR and a TSX dataset (background image is a Google Map). (c) Dynamic structural behaviors of the bridge measured with GPRI-II system [159]. The bar figures on the positions of L, J, and H represent the maximum vertical motion recorded with GPS when different trains were passing.

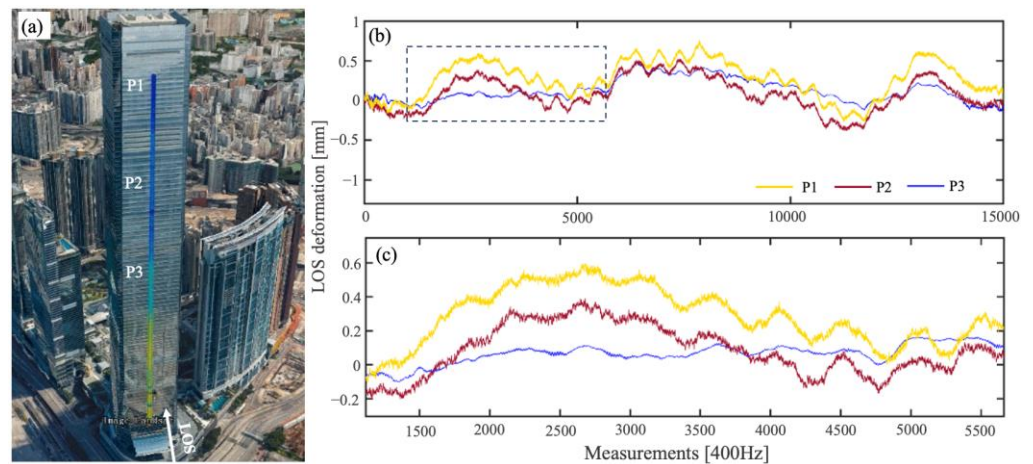


Figure 25. LOS deformation of a high-rise building in Hong Kong (a). The time series of selected points with different positions (b). The enlarged display of part of time series (c).

5.2. Future Work

According to the previous discussion, the radar interferometric techniques of both spaceborne InSAR and GBRI can be further enhanced by utilizing the following aspects to monitor urban infrastructures more effectively:

- **Optimized strategy for radar measurements selection:** To enhance the distribution of radar measurements and mitigate the reliance on specific thresholds (see Section 5.1.1), it is advisable to connect the final deformation product requirements with detectable measurement points. For example, monitoring ground deformation caused by activities such as groundwater pumping or engineering construction requires different monitoring accuracy requirements. Therefore, the distribution of usable or detectable measurements points in terms of radar observation quality will change accordingly. In addition, the combined use of multiple radar systems, spaceborne or ground-based, presents an opportunity to improve the integrity of radar measurements in dense ur-

ban built-up areas. The integration helps overcome geometric distortions and ensures more complete coverage of the target area.

- Deformation in a rapid urbanization area: The rapid processes of urbanization and urban renewal bring about substantial changes to ground features, resulting in fast decorrelation effects in radar interferometry techniques. It is difficult to maintain the radar interferometry coherence over time, and obtaining ground deformation over a long time in such areas presents significant challenges. It is crucial to develop techniques that can effectively capture ground deformations during the rapid decorrelation periods, as this would provide valuable information. Initial research has been carried out on the exploration of the temporary PS points in [217].
- Development of advanced models and methods: Developing advanced methods is crucial to accurately detect deformation characteristics in urban areas. Tailored techniques such as advanced phase unwrapping can improve measurement quality while compensating for atmospheric effects enhances deformation accuracy. Additionally, different infrastructures in urban areas have varying deformation characteristics. By combining engineering models, we can differentiate between normal deformation and anomalous deformation, leading to improved detection accuracy. Furthermore, integrating engineering models to interpret measurement results, such as establishing the normal range of deformation for a structure, is crucial.
- Efficient data processing strategies: Efficient data processing is crucial for long-term urban infrastructure monitoring. To achieve this, more efficient processing methods for both spaceborne and ground-based systems should be investigated and adopted, e.g., sequential estimators [211,218]. These methods should facilitate timely updates of interferometric measurements as new data become available. This is especially vital when dealing with extensive study areas with large SAR datasets. In addition, precise repositioning of the GBRI system is also essential for long-term deformation monitoring as discussed in Section 2 [105,106,219]. If the instrument pillar cannot be built to maintain a stable observation position, it is very important to develop repositioning error correction methods to ensure accuracy.
- Improved interpretation of deformation products: Radar interferometry provides valuable information about infrastructure deformation, but the interpretation of results can be nonintuitive, hindering its proper utilization, especially among non-experts. Enhancing the interpretation and data mining of deformation results with multi-disciplinary knowledge can improve understanding. The development of artificial intelligence (AI) techniques for the automatic interpretation of deformation data can make them more accessible to a wider audience and facilitate effective utilization; similar research has been carried out in geohazard monitoring [220,221].

6. Conclusions

Urban infrastructures play a critical role in supporting the lives of urban dwellers. Regular monitoring of the deformation and dynamic behaviors of urban infrastructures is necessary to identify potential risks such as structural failures. Radar interferometry, as a powerful geodetic technique, has been widely used in monitoring the stability conditions of urban infrastructures due to its wide coverage, high spatial resolution, and accurate deformation measurements. In this paper, we have provided a comprehensive review of radar interferometric techniques (including both spaceborne InSAR and GBRI techniques) and their recent advancements with a special emphasis on the applications in urban infrastructure deformation monitoring. The following are the main contributions from this review:

- (1) Both spaceborne InSAR and GBRI have been widely used for the urban infrastructure deformation monitoring. The applications have been increasing over the recent decades, in particular over the recent 10 years.
- (2) Recent advances and applications of both spaceborne InSAR and GBRI techniques in urban infrastructure deformation monitoring were discussed. These include multi-

dimensional deformation monitoring, multi-platform SAR datasets, anomalous deformation detection, accurate 3D geolocation of measurements, general survey of urban surface deformation, and surveillance of infrastructure stability.

- (3) Several challenges in monitoring urban infrastructure deformation using radar interferometry were identified. These include the inconsistency in the distribution of selected measurements from different methods, difficulties in phase unwrapping in urban areas, rapid decorrelation, geometric distortions, and technology selection in monitoring highly dynamic infrastructures. The potential future research directions in both spaceborne InSAR and GBRI for infrastructure deformation monitoring were also discussed, including an optimization strategy for radar measurements selection, long-term deformation monitoring, monitoring deformation in areas of rapid urbanization and geometric distortions, efficient data processing strategies, and better interpretation of deformation measurement results.

Author Contributions: Conceptualization, S.W., B.Z. and X.D.; methodology, S.W. and Z.Z. (Zhijie Zhang); validation, B.Z. and S.W.; investigation, X.D. and L.Z.; resources, S.W., B.Z. and Z.Z. (Zeyu Zhang); data curation, S.W. and B.Z.; writing—original draft preparation, S.W. and B.Z.; writing—review and editing, S.W., B.Z. and X.D.; supervision, X.D. and L.Z.; funding acquisition, S.W., B.Z. and X.D. All authors have read and agreed to the published version of the manuscript.

Funding: This work was supported by the Research Grants Council of Hong Kong (PolyU 152233/19E, PolyU 152318/22E, PolyU 152344/23E), the University Grants Council of the Hong Kong Polytechnic University (1-BD2S), the Innovation and Technology Fund of Hong Kong (ITP/019/20LP), the Guangdong Basic and Applied Basic Research Foundation (No. 2021A1515011427), and the National Natural Science Foundation of China (Grant 42304014).

Institutional Review Board Statement: Not applicable.

Informed Consent Statement: Not applicable.

Data Availability Statement: The CSK data is provided by the E-GEOS under project ID 703, the TSX data is provided by the DLR under project GEO 3603, and the Sentinel-1A data is free available from the ESA. The ground-based radar data is achieved by the GPRI-II system bought by The Hong Kong Polytechnic University.

Acknowledgments: The authors would like to thank the editors and reviewers for providing constructive suggestions for improving this manuscript.

Conflicts of Interest: The authors declare no conflict of interest.

References

- O'Neill, M.W.; Sarhan, H.A. Structural resistance factors for drilled shafts considering construction flaws. In *Current Practices and Future Trends in Deep Foundations*; ASCE Library: Lawrence, KS, USA, 2004; pp. 166–185.
- Khotamov, A.T. Influence of the Intensity of Physical Wear and Tear on the Durability of Multi-Apartment Residential Buildings. *Ann. For. Res.* **2022**, *65*, 9839–9848.
- McCall, G. Geohazards and the urban environment. *Geol. Soc. Lond. Eng. Geol. Spec. Publ.* **1998**, *15*, 309–318. [[CrossRef](#)]
- Bianchini, S.; Pratesi, F.; Nolesini, T.; Casagli, N. Building deformation assessment by means of persistent scatterer interferometry analysis on a landslide-affected area: The Volterra (Italy) case study. *Remote Sens.* **2015**, *7*, 4678–4701. [[CrossRef](#)]
- Brinkmann, R.; Parise, M.; Dye, D. Sinkhole distribution in a rapidly developing urban environment: Hillsborough County, Tampa Bay area, Florida. *Eng. Geol.* **2008**, *99*, 169–184. [[CrossRef](#)]
- Hunter, G.; Fell, R. *The Deformation Behaviour of Embankment Dams*; University of New South Wales, School of Civil and Environmental Engineering: Sydney, NSW, Australia, 2003.
- Sony, S.; Laventure, S.; Sadhu, A. A literature review of next-generation smart sensing technology in structural health monitoring. *Struct. Control Health Monit.* **2019**, *26*, e2321. [[CrossRef](#)]
- Ansari, F. *Sensing Issues in Civil Structural Health Monitoring*; Springer: Berlin/Heidelberg, Germany, 2005; Volume 1.
- Pratesi, F.; Tapete, D.; Terenzi, G.; Del Ventisette, C.; Moretti, S. Rating health and stability of engineering structures via classification indexes of InSAR Persistent Scatterers. *Int. J. Appl. Earth Obs. Geoinf.* **2015**, *40*, 81–90. [[CrossRef](#)]
- Giardina, G.; Milillo, P.; DeJong, M.J.; Perissin, D.; Milillo, G. Evaluation of InSAR monitoring data for post-tunnelling settlement damage assessment. *Struct. Control Health Monit.* **2019**, *26*, e2285. [[CrossRef](#)]

11. Milillo, P.; Perissin, D.; Salzer, J.T.; Lundgren, P.; Lacava, G.; Milillo, G.; Serio, C. Monitoring dam structural health from space: Insights from novel InSAR techniques and multi-parametric modeling applied to the Pertusillo dam Basilicata, Italy. *Int. J. Appl. Earth Obs. Geoinf.* **2016**, *52*, 221–229. [[CrossRef](#)]
12. Chang, L. Monitoring Civil Infrastructure Using Satellite Radar Interferometry. Ph.D. Thesis, Delft University of Technology, Delft, The Netherlands, 2015.
13. Strozzi, T.; Wegmuller, U.; Werner, C.; Wiesmann, A. Measurement of slow uniform surface displacement with mm/year accuracy. In *IGARSS 2000, Proceedings of the IEEE 2000 International Geoscience and Remote Sensing Symposium, Taking the Pulse of the Planet: The Role of Remote Sensing in Managing the Environment, Honolulu, HI, USA, 24–28 July 2000*; Proceedings (Cat. No. 00CH37120); IEEE: Piscataway, NJ, USA; pp. 2239–2241.
14. Ferretti, A.; Savio, G.; Barzaghi, R.; Borghi, A.; Musazzi, S.; Novali, F.; Prati, C.; Rocca, F. Submillimeter accuracy of InSAR time series: Experimental validation. *IEEE Trans. Geosci. Remote Sens.* **2007**, *45*, 1142–1153. [[CrossRef](#)]
15. Ghuman, B.T.R.a.P. Automated generation of near realtime, optimum accuracy movement products with Sentinel-1A IW data. In Proceedings of the FRINGE 15 Meeting, Frascati, Italy, 23–27 March 2015.
16. Wasowski, J.; Pisano, L. Long-term InSAR, borehole inclinometer, and rainfall records provide insight into the mechanism and activity patterns of an extremely slow urbanized landslide. *Landslides* **2020**, *17*, 445–457. [[CrossRef](#)]
17. Bennett, A.; Blacknell, D. Infrastructure analysis from high resolution SAR and InSAR imagery. In Proceedings of the 2003 2nd GRSS/ISPRS Joint Workshop on Remote Sensing and Data Fusion over Urban Areas, Berlin, Germany, 22–23 May 2003; pp. 230–235.
18. Lin, H.; Ma, P.; Wang, W. Urban Infrastructure Health Monitoring with Spaceborne Multi-temporal Synthetic Aperture Radar Interferometry. *Acta Geod. Cartogr. Sin.* **2017**, *46*, 1421–1433.
19. Crosetto, M.; Monserrat, O.; Herrera, G. Urban applications of persistent scatterer interferometry. In *Radar Remote Sensing of Urban Areas*; Springer: Berlin/Heidelberg, Germany, 2010; pp. 233–248.
20. Peduto, D.; Oricchio, L.; Nicodemo, G.; Crosetto, M.; Ripoll, J.; Buxó, P.; Janeras, M. Investigating the kinematics of the unstable slope of Barberà de la Conca (Catalonia, Spain) and the effects on the exposed facilities by GBSAR and multi-source conventional monitoring. *Landslides* **2021**, *18*, 457–469. [[CrossRef](#)]
21. Noferini, L.; Pieraccini, M.; Mecatti, D.; Macaluso, G.; Atzeni, C.; Mantovani, M.; Marcato, G.; Pasuto, A.; Silvano, S.; Tagliavini, F. Using GB-SAR technique to monitor slow moving landslide. *Eng. Geol.* **2007**, *95*, 88–98. [[CrossRef](#)]
22. Kuras, P.; Ortyl, Ł.; Owerko, T.; Salamak, M.; Łaziński, P. GB-SAR in the diagnosis of critical city infrastructure—A case study of a load test on the long tram extradosed bridge. *Remote Sens.* **2020**, *12*, 3361. [[CrossRef](#)]
23. Ma, P.; Lin, H.; Wang, W.; Yu, H.; Chen, F.; Jiang, L.; Zhou, L.; Zhang, Z.; Shi, G.; Wang, J. Toward Fine Surveillance: A Review of Multitemporal Interferometric Synthetic Aperture Radar for Infrastructure Health Monitoring. *IEEE Geosci. Remote Sens. Mag.* **2021**, *10*, 207–230. [[CrossRef](#)]
24. Monserrat, O.; Crosetto, M.; Luzi, G. A review of ground-based SAR interferometry for deformation measurement. *ISPRS J. Photogramm. Remote Sens.* **2014**, *93*, 40–48. [[CrossRef](#)]
25. Skolnik, M.I. *Introduction to Radar Systems*; McGraw-Hill Education: New York, NY, USA, 1980.
26. Bamler, R. Principles of synthetic aperture radar. *Surv. Geophys.* **2000**, *21*, 147–157. [[CrossRef](#)]
27. Massonnet, D.; Souyris, J.-C. *Imaging with Synthetic Aperture Radar*; EPFL Press: Lausanne, Switzerland, 2008.
28. Oliver, C.; Quegan, S. *Understanding Synthetic Aperture Radar Images*; SciTech Publishing: Chennai, India, 2004.
29. Bamler, R.; Hartl, P. Synthetic aperture radar interferometry. *Inverse Probl.* **1998**, *14*, R1. [[CrossRef](#)]
30. Massonnet, D.; Feigl, K.L. Radar interferometry and its application to changes in the Earth's surface. *Rev. Geophys.* **1998**, *36*, 441–500. [[CrossRef](#)]
31. Hanssen, R.F. *Radar Interferometry: Data Interpretation and Error Analysis*; Springer Science & Business Media: Berlin/Heidelberg, Germany, 2001; Volume 2.
32. Hanssen, R.; Bamler, R. Evaluation of interpolation kernels for SAR interferometry. *IEEE Trans. Geosci. Remote Sens.* **1999**, *37*, 318–321. [[CrossRef](#)]
33. Li, Z.; Bethel, J. Image coregistration in SAR interferometry. The International Archives of the Photogrammetry. *Remote Sens. Spat. Inf. Sci.* **2008**, *37*, 433–438.
34. Pepe, A.; Solaro, G.; Calo, F.; Dema, C. A minimum acceleration approach for the retrieval of multiplatform InSAR deformation time series. *IEEE J. Sel. Top. Appl. Earth Obs. Remote Sens.* **2016**, *9*, 3883–3898. [[CrossRef](#)]
35. Zebker, H.A.; Goldstein, R.M. Topographic mapping from interferometric synthetic aperture radar observations. *J. Geophys. Res. Solid Earth* **1986**, *91*, 4993–4999. [[CrossRef](#)]
36. Goldstein, R.M.; Zebker, H.A.; Werner, C.L. Satellite radar interferometry: Two-dimensional phase unwrapping. *Radio Sci.* **1988**, *23*, 713–720. [[CrossRef](#)]
37. Costantini, M. A novel phase unwrapping method based on network programming. *IEEE Trans. Geosci. Remote Sens.* **1998**, *36*, 813–821. [[CrossRef](#)]
38. Bock, Y.; Williams, S. Integrated satellite interferometry in southern California. *Eos Trans. Am. Geophys. Union* **1997**, *78*, 293–300. [[CrossRef](#)]
39. Klees, R.; Massonnet, D. Deformation measurements using SAR interferometry: Potential and limitations. *Geol. Mijnb.* **1999**, *77*, 161–176. [[CrossRef](#)]

40. Beauducel, F.; Briole, P.; Froger, J.L. Volcano-wide fringes in ERS synthetic aperture radar interferograms of Etna (1992–1998): Deformation or tropospheric effect? *J. Geophys. Res. Solid Earth* **2000**, *105*, 16391–16402. [[CrossRef](#)]
41. Hanssen, R.; Moisseev, D.; Businger, S. Resolving the acquisition ambiguity for atmospheric monitoring in multi-pass radar interferometry. In *IGARSS 2003, Proceedings of the 2003 IEEE International Geoscience and Remote Sensing Symposium, Toulouse, France, 21–25 July 2003*; Proceedings (IEEE Cat. No.03CH37477); IEEE: Piscataway, NJ, USA; pp. 1202–1205.
42. Simons, M.; Fialko, Y.; Rivera, L. Coseismic deformation from the 1999 Mw 7.1 Hector Mine, California, earthquake as inferred from InSAR and GPS observations. *Bull. Seismol. Soc. Am.* **2002**, *92*, 1390–1402. [[CrossRef](#)]
43. Sandwell, D.T.; Price, E.J. Phase gradient approach to stacking interferograms. *J. Geophys. Res. Solid Earth* **1998**, *103*, 30183–30204. [[CrossRef](#)]
44. Ferretti, A.; Prati, C.; Rocca, F. Nonlinear subsidence rate estimation using permanent scatterers in differential SAR interferometry. *IEEE Trans. Geosci. Remote Sens.* **2000**, *38*, 2202–2212. [[CrossRef](#)]
45. Ferretti, A.; Prati, C.; Rocca, F. Permanent scatterers in SAR interferometry. *IEEE Trans. Geosci. Remote Sens.* **2001**, *39*, 8–20. [[CrossRef](#)]
46. Berardino, P.; Fornaro, G.; Lanari, R.; Sansosti, E. A new algorithm for surface deformation monitoring based on small baseline differential SAR interferograms. *IEEE Trans. Geosci. Remote Sens.* **2002**, *40*, 2375–2383. [[CrossRef](#)]
47. Hooper, A. A multi-temporal InSAR method incorporating both persistent scatterer and small baseline approaches. *Geophys. Res. Lett.* **2008**, *35*, L16302. [[CrossRef](#)]
48. Ferretti, A.; Fumagalli, A.; Novali, F.; Prati, C.; Rocca, F.; Rucci, A. A new algorithm for processing interferometric data-stacks: SqueeSAR. *IEEE Trans. Geosci. Remote Sens.* **2011**, *49*, 3460–3470. [[CrossRef](#)]
49. Werner, C.; Wegmüller, U.; Strozzi, T.; Wiesmann, A. Interferometric point target analysis for deformation mapping. In *IGARSS 2003, Proceedings of the 2003 IEEE International Geoscience and Remote Sensing Symposium, Toulouse, France, 21–25 July 2003*; Proceedings (IEEE Cat. No.03CH37477); IEEE: Piscataway, NJ, USA; pp. 4362–4364.
50. Zhang, L.; Ding, X.; Lu, Z. Ground settlement monitoring based on temporarily coherent points between two SAR acquisitions. *ISPRS J. Photogramm. Remote Sens.* **2011**, *66*, 146–152. [[CrossRef](#)]
51. Hooper, A.; Zebker, H.; Segall, P.; Kampes, B. A new method for measuring deformation on volcanoes and other natural terrains using InSAR persistent scatterers. *Geophys. Res. Lett.* **2004**, *31*, L23611. [[CrossRef](#)]
52. Li, T.; Liu, G.; Lin, H.; Jia, H.; Zhang, R.; Yu, B.; Luo, Q. A hierarchical multi-temporal InSAR method for increasing the spatial density of deformation measurements. *Remote Sens.* **2014**, *6*, 3349–3368. [[CrossRef](#)]
53. Ojha, C.; Manunta, M.; Lanari, R.; Pepe, A. The Constrained-Network Propagation (C-NetP) Technique to Improve SBAS-DInSAR Deformation Time Series Retrieval. *IEEE J. Sel. Top. Appl. Earth Obs. Remote Sens.* **2015**, *8*, 4910–4921. [[CrossRef](#)]
54. Kampes, B.M. *Radar Interferometry*; Springer: Berlin/Heidelberg, Germany, 2006.
55. Pepe, A.; Lanari, R. On the extension of the minimum cost flow algorithm for phase unwrapping of multitemporal differential SAR interferograms. *IEEE Trans. Geosci. Remote Sens.* **2006**, *44*, 2374–2383. [[CrossRef](#)]
56. Zhang, L.; Ding, X.; Lu, Z. Modeling PSInSAR time series without phase unwrapping. *IEEE Trans. Geosci. Remote Sens.* **2011**, *49*, 547–556. [[CrossRef](#)]
57. Flynn, T.J. Two-dimensional phase unwrapping with minimum weighted discontinuity. *JOSA A* **1997**, *14*, 2692–2701. [[CrossRef](#)]
58. Ghiglia, D.C.; Romero, L.A. Robust two-dimensional weighted and unweighted phase unwrapping that uses fast transforms and iterative methods. *JOSA A* **1994**, *11*, 107–117. [[CrossRef](#)]
59. Fattahi, H.; Amelung, F. DEM error correction in InSAR time series. *IEEE Trans. Geosci. Remote Sens.* **2013**, *51*, 4249–4259. [[CrossRef](#)]
60. Chang, L.; Hanssen, R.F. A probabilistic approach for InSAR time-series postprocessing. *IEEE Trans. Geosci. Remote Sens.* **2015**, *54*, 421–430. [[CrossRef](#)]
61. Baehr, H. *Orbital Effects in Spaceborne Synthetic Aperture Radar Interferometry*; KIT Scientific Publishing: Karlsruhe, Deutschland, 2013.
62. Fattahi, H.; Amelung, F. InSAR uncertainty due to orbital errors. *Geophys. J. Int.* **2014**, *199*, 549–560. [[CrossRef](#)]
63. Mancon, S.; Guarnieri, A.M.; Tebaldini, S.; Giudici, D. Orbital error estimation through multi-squint analysis. In *EUSAR 2014, Proceedings of the 10th European Conference on Synthetic Aperture Radar, Berlin, Germany, 3–5 June 2014*; IEEE: Piscataway, NJ, USA; pp. 1–4.
64. Zhang, L.; Ding, X.; Lu, Z.; Jung, H.-S.; Hu, J.; Feng, G. A novel multitemporal InSAR model for joint estimation of deformation rates and orbital errors. *IEEE Trans. Geosci. Remote Sens.* **2014**, *52*, 3529–3540. [[CrossRef](#)]
65. Cao, Y.; Li, Z.; Wei, J.; Hu, J.; Duan, M.; Feng, G. Stochastic modeling for time series InSAR: With emphasis on atmospheric effects. *J. Geod.* **2018**, *92*, 185–204. [[CrossRef](#)]
66. Yu, C.; Li, Z.; Penna, N.T.; Crippa, P. Generic atmospheric correction model for Interferometric Synthetic Aperture Radar observations. *J. Geophys. Res. Solid Earth* **2018**, *123*, 9202–9222. [[CrossRef](#)]
67. Liang, H.; Zhang, L.; Lu, Z.; Li, X. Correction of spatially varying stratified atmospheric delays in multitemporal InSAR. *Remote Sens. Environ.* **2023**, *285*, 113382. [[CrossRef](#)]
68. Duan, M.; Xu, B.; Li, Z.; Wu, W.; Cao, Y.; Liu, J.; Wang, G.; Hou, J. A new weighting method by considering the physical characteristics of atmospheric turbulence and decorrelation noise in SBAS-InSAR. *Remote Sens.* **2020**, *12*, 2557. [[CrossRef](#)]

69. Crosetto, M.; Devanthery, N.; Monserrat, O.; Barra, A.; Cuevas-González, M.; Mróz, M.; Botey-Bassols, J.; Vázquez-Suñé, E.; Crippa, B. A persistent scatterer interferometry procedure based on stable areas to filter the atmospheric component. *Remote Sens.* **2018**, *10*, 1780. [[CrossRef](#)]
70. Jung, H.-S.; Lee, D.-T.; Lu, Z.; Won, J.-S. Ionospheric correction of SAR interferograms by multiple-aperture interferometry. *IEEE Trans. Geosci. Remote Sens.* **2012**, *51*, 3191–3199. [[CrossRef](#)]
71. Gomba, G.; Parizzi, A.; De Zan, F.; Eineder, M.; Bamler, R. Toward operational compensation of ionospheric effects in SAR interferograms: The split-spectrum method. *IEEE Trans. Geosci. Remote Sens.* **2015**, *54*, 1446–1461. [[CrossRef](#)]
72. Zhang, B.; Wang, C.; Ding, X.; Zhu, W.; Wu, S. Correction of ionospheric artifacts in SAR data: Application to fault slip inversion of 2009 Southern Sumatra Earthquake. *IEEE Geosci. Remote Sens. Lett.* **2018**, *15*, 1327–1331. [[CrossRef](#)]
73. Zhang, B.; Ding, X.; Amelung, F.; Wang, C.; Xu, W.; Zhu, W.; Shimada, M.; Zhang, Q.; Baba, T. Impact of ionosphere on InSAR observation and coseismic slip inversion: Improved slip model for the 2010 Maule, Chile, earthquake. *Remote Sens. Environ.* **2021**, *267*, 112733. [[CrossRef](#)]
74. Liang, H.; Zhang, L.; Lu, Z.; Li, X. Nonparametric Estimation of DEM Error in Multitemporal InSAR. *IEEE Trans. Geosci. Remote Sens.* **2019**, *57*, 10004–10014. [[CrossRef](#)]
75. Zhang, W.; Zhu, W.; Tian, X.; Zhang, Q.; Zhao, C.; Niu, Y.; Wang, C. Improved DEM Reconstruction Method Based on Multibaseline InSAR. *IEEE Geosci. Remote Sens. Lett.* **2021**, *19*, 4011505. [[CrossRef](#)]
76. Wang, T.; Jónsson, S.; Hanssen, R.F. Improved SAR image coregistration using pixel-offset series. *IEEE Geosci. Remote Sens. Lett.* **2014**, *11*, 1465–1469. [[CrossRef](#)]
77. Natsuaki, R.; Hirose, A. InSAR local co-registration method assisted by shape-from-shading. *IEEE J. Sel. Top. Appl. Earth Obs. Remote Sens.* **2012**, *6*, 953–959. [[CrossRef](#)]
78. Refice, A.; Bovenga, F.; Nutricato, R. MST-based stepwise connection strategies for multipass radar data, with application to coregistration and equalization. *IEEE Trans. Geosci. Remote Sens.* **2006**, *44*, 2029–2040. [[CrossRef](#)]
79. Xu, B.; Li, Z.; Zhu, Y.; Shi, J.; Feng, G. Kinematic coregistration of sentinel-1 TOPSAR images based on sequential least squares adjustment. *IEEE J. Sel. Top. Appl. Earth Obs. Remote Sens.* **2020**, *13*, 3083–3093. [[CrossRef](#)]
80. Pinel-Puysségur, B.; Lasserre, C.; Benoit, A.; Jolivet, R.; Doin, M.-P.; Champenois, J. A simple phase unwrapping errors correction algorithm based on phase closure analysis. In Proceedings of the IGARSS 2018–2018 IEEE International Geoscience and Remote Sensing Symposium, Valencia, Spain, 22–27 July 2018; pp. 2212–2215.
81. Zhang, Y.; Heresh, F.; Falk, A. Small baseline InSAR time series analysis: Unwrapping error correction and noise reduction. *Comput. Geosci.* **2019**, *133*, 104331.
82. Wu, S.; Zhang, B.; Ding, X.; Shahzad, N.; Zhang, L.; Lu, Z. A hybrid method for MT-InSAR phase unwrapping for deformation monitoring in urban areas. *Int. J. Appl. Earth Obs. Geoinf.* **2022**, *112*, 102963. [[CrossRef](#)]
83. Yang, M.; Dheenathayalan, P.; López-Dekker, P.; van Leijen, F.; Liao, M.; Hanssen, R.F. On the influence of sub-pixel position correction for PS localization accuracy and time series quality. *ISPRS J. Photogramm. Remote Sens.* **2020**, *165*, 98–107. [[CrossRef](#)]
84. Yang, M.; López-Dekker, P.; Dheenathayalan, P.; Liao, M.; Hanssen, R.F. On the value of corner reflectors and surface models in InSAR precise point positioning. *ISPRS J. Photogramm. Remote Sens.* **2019**, *158*, 113–122. [[CrossRef](#)]
85. Hooper, A.J. *Persistent Scatter Radar Interferometry for Crustal Deformation Studies and Modeling of Volcanic Deformation*; Stanford University: Stanford, CA, USA, 2006.
86. Blanco-Sánchez, P.; Mallorquí, J.J.; Duque, S.; Monells, D. The Coherent Pixels Technique (CPT): An Advanced DInSAR Technique for Nonlinear Deformation Monitoring. In *Earth Sciences and Mathematics: Volume 1*; Camacho, A.G., Díaz, J.I., Fernández, J., Eds.; Birkhäuser Basel: Basel, Switzerland, 2008; pp. 1167–1193.
87. Costantini, M.; Falco, S.; Malvarosa, F.; Minati, F.; Trillo, F.; Vecchioli, F. Persistent scatterer pair interferometry: Approach and application to COSMO-SkyMed SAR data. *IEEE J. Sel. Top. Appl. Earth Obs. Remote Sens.* **2014**, *7*, 2869–2879. [[CrossRef](#)]
88. Wu, S.; Zhang, L.; Ding, X.; Perissin, D. Pixel-Wise MTInSAR Estimator for Integration of Coherent Point Selection and Unwrapped Phase Vector Recovery. *IEEE Trans. Geosci. Remote Sens.* **2019**, *57*, 2659–2668. [[CrossRef](#)]
89. Fornaro, G.; Verde, S.; Reale, D.; Pauciuillo, A. CAESAR: An approach based on covariance matrix decomposition to improve multibaseline–multitemporal interferometric SAR processing. *IEEE Trans. Geosci. Remote Sens.* **2015**, *53*, 2050–2065. [[CrossRef](#)]
90. Dong, J.; Zhang, L.; Tang, M.; Liao, M.; Xu, Q.; Gong, J.; Ao, M. Mapping landslide surface displacements with time series SAR interferometry by combining persistent and distributed scatterers: A case study of Jiaju landslide in Danba, China. *Remote Sens. Environ.* **2018**, *205*, 180–198. [[CrossRef](#)]
91. Lazecký, M.; Spaans, K.; González, P.J.; Maghsoudi, Y.; Morishita, Y.; Albino, F.; Elliott, J.; Greenall, N.; Hatton, E.; Hooper, A. LiCSAR: An automatic InSAR tool for measuring and monitoring tectonic and volcanic activity. *Remote Sens.* **2020**, *12*, 2430. [[CrossRef](#)]
92. Zhu, X.X.; Bamler, R. Very high resolution spaceborne SAR tomography in urban environment. *IEEE Trans. Geosci. Remote Sens.* **2010**, *48*, 4296–4308. [[CrossRef](#)]
93. Perissin, D.; Wang, T. Repeat-pass SAR interferometry with partially coherent targets. *IEEE Trans. Geosci. Remote Sens.* **2012**, *50*, 271–280. [[CrossRef](#)]
94. Caduff, R.; Schlunegger, F.; Kos, A.; Wiesmann, A. A review of terrestrial radar interferometry for measuring surface change in the geosciences. *Earth Surf. Process. Landf.* **2015**, *40*, 208–228. [[CrossRef](#)]
95. Pieraccini, M.; Miccinesi, L. Ground-based radar interferometry: A bibliographic review. *Remote Sens.* **2019**, *11*, 1029. [[CrossRef](#)]

96. Luzi, G.; Pieraccini, M.; Mecatti, D.; Noferini, L.; Guidi, G.; Moia, F.; Atzeni, C. Ground-based radar interferometry for landslides monitoring: Atmospheric and instrumental decorrelation sources on experimental data. *IEEE Trans. Geosci. Remote Sens.* **2004**, *42*, 2454–2466. [[CrossRef](#)]
97. Zheng, X.; Yang, X.; Ma, H.; Ren, G.; Zhang, K.; Yang, F.; Li, C. Integrated ground-based SAR interferometry, terrestrial laser scanner, and corner reflector deformation experiments. *Sensors* **2018**, *18*, 4401. [[CrossRef](#)]
98. Deng, Y.; Tian, W.; Xiao, T.; Hu, C.; Yang, H. High-Quality Pixel Selection Applied for Natural Scenes in GB-SAR Interferometry. *Remote Sens.* **2021**, *13*, 1617. [[CrossRef](#)]
99. Chao, B.; Zhang, D.; Huang, H. An overview of atmospheric correction for GB-SAR. In Proceedings of the 2019 IEEE 19th International Conference on Communication Technology (ICCT), Xi'an, China, 16–19 October 2019; pp. 1062–1072.
100. Owerko, T.; Kuras, P.; Ortyl, Ł. Atmospheric correction thresholds for ground-based radar interferometry deformation monitoring estimated using time series analyses. *Remote Sens.* **2020**, *12*, 2236. [[CrossRef](#)]
101. Wang, Z.; Li, Z.; Mills, J. A new approach to selecting coherent pixels for ground-based SAR deformation monitoring. *ISPRS J. Photogramm. Remote Sens.* **2018**, *144*, 412–422. [[CrossRef](#)]
102. Hu, C.; Deng, Y.; Tian, W.; Wang, J. A PS processing framework for long-term and real-time GB-SAR monitoring. *Int. J. Remote Sens.* **2019**, *40*, 6298–6314. [[CrossRef](#)]
103. Yang, H.; Liu, J.; Peng, J.; Wang, J.; Zhao, B.; Zhang, B. A method for GB-InSAR temporal analysis considering the atmospheric correlation in time series. *Nat. Hazards* **2020**, *104*, 1465–1480. [[CrossRef](#)]
104. Beni, A.; Miccinesi, L.; Michelini, A.; Pieraccini, M. Temporal coherence estimators for GBSAR. *Remote Sens.* **2022**, *14*, 3039. [[CrossRef](#)]
105. Wang, Z.; Li, Z.; Mills, J. Modelling of instrument repositioning errors in discontinuous Multi-Campaign Ground-Based SAR (MC-GBSAR) deformation monitoring. *ISPRS J. Photogramm. Remote Sens.* **2019**, *157*, 26–40. [[CrossRef](#)]
106. Hu, C.; Zhu, J.; Deng, Y.; Tian, W.; Yin, P. Repositioning error compensation in discontinuous ground-based SAR monitoring. *Remote Sens.* **2021**, *13*, 2461. [[CrossRef](#)]
107. Yang, H.; Cai, J.; Peng, J.; Wang, J.; Jiang, Q. A correcting method about GB-SAR rail displacement. *Int. J. Remote Sens.* **2017**, *38*, 1483–1493. [[CrossRef](#)]
108. Lei, T.; Wang, J.; Huang, P.; Tan, W.; Qi, Y.; Xu, W.; Zhao, C. Time-varying baseline error correction method for ground-based micro-deformation monitoring radar. *J. Syst. Eng. Electron.* **2022**, *33*, 938–950. [[CrossRef](#)]
109. Takahashi, K.; Matsumoto, M.; Sato, M. Continuous observation of natural-disaster-affected areas using ground-based SAR interferometry. *IEEE J. Sel. Top. Appl. Earth Obs. Remote Sens.* **2013**, *6*, 1286–1294. [[CrossRef](#)]
110. Di Pasquale, A.; Corsetti, M.; Guccione, P.; Lugli, A.; Nicoletti, M.; Nico, G.; Zonno, M. Ground-based SAR interferometry as a supporting tool in natural and man-made disasters. In Proceedings of the 33rd EARSel Symposium, Matera, Italy, 3–6 June 2013; pp. 3–6.
111. Xing, C.; Yu, Z.; Zhou, X.; Wang, P. Research on the testing methods for IBIS-S system. In *IOP Conference Series: Earth and Environmental Science*; IOP Publishing: Bristol, UK, 2014; p. 012263.
112. Kuras, P.; Ortyl, Ł.; Owerko, T. Empirical SNR-based model of the displacement accuracy for ground-based radar measurements. *ISPRS J. Photogramm. Remote Sens.* **2022**, *194*, 181–194. [[CrossRef](#)]
113. Wright, T.J.; Parsons, B.E.; Lu, Z. Toward mapping surface deformation in three dimensions using InSAR. *Geophys. Res. Lett.* **2004**, *31*, L01607. [[CrossRef](#)]
114. Hu, J.; Li, Z.; Ding, X.; Zhu, J.; Zhang, L.; Sun, Q. Resolving three-dimensional surface displacements from InSAR measurements: A review. *Earth-Sci. Rev.* **2014**, *133*, 1–17. [[CrossRef](#)]
115. Sun, Q.; Hu, J.; Zhang, L.; Ding, X. Towards slow-moving landslide monitoring by integrating multi-sensor InSAR time series datasets: The Zhouqu case study, China. *Remote Sens.* **2016**, *8*, 908. [[CrossRef](#)]
116. Ouchi, K. Recent trend and advance of synthetic aperture radar with selected topics. *Remote Sens.* **2013**, *5*, 716–807. [[CrossRef](#)]
117. Osmanoglu, B.; Sunar, F.; Wdowinski, S.; Cabral-Cano, E. Time series analysis of InSAR data: Methods and trends. *ISPRS J. Photogramm. Remote Sens.* **2016**, *115*, 90–102. [[CrossRef](#)]
118. Bhattacharya, A.; Mukherjee, K. Review on InSAR based displacement monitoring of Indian Himalayas: Issues, challenges and possible advanced alternatives. *Geocarto Int.* **2017**, *32*, 298–321. [[CrossRef](#)]
119. Casu, F.; Manunta, M.; Agram, P.; Crippen, R. Big Remotely Sensed Data: Tools, applications and experiences. *Remote Sens. Environ.* **2017**, *202*, 1–2. [[CrossRef](#)]
120. Pepe, A.; Calò, F. A review of interferometric synthetic aperture RADAR (InSAR) multi-track approaches for the retrieval of Earth's surface displacements. *Appl. Sci.* **2017**, *7*, 1264. [[CrossRef](#)]
121. Even, M.; Schulz, K. InSAR deformation analysis with distributed scatterers: A review complemented by new advances. *Remote Sens.* **2018**, *10*, 744. [[CrossRef](#)]
122. Ge, P.; Gokon, H.; Meguro, K. A review on synthetic aperture radar-based building damage assessment in disasters. *Remote Sens. Environ.* **2020**, *240*, 111693. [[CrossRef](#)]
123. Minh, D.H.T.; Hanssen, R.; Rocca, F. Radar Interferometry: 20 Years of Development in Time Series Techniques and Future Perspectives. *Remote Sens.* **2020**, *12*, 1364. [[CrossRef](#)]
124. Zhang, L.; Ding, X.; Lu, Z. Ground deformation mapping by fusion of multi-temporal interferometric synthetic aperture radar images: A review. *Int. J. Image Data Fusion* **2015**, *6*, 289–313. [[CrossRef](#)]

125. Crosetto, M.; Monserrat, O.; Cuevas-González, M.; Devanthery, N.; Crippa, B. Persistent scatterer interferometry: A review. *ISPRS J. Photogramm. Remote Sens.* **2016**, *115*, 78–89. [[CrossRef](#)]
126. Yang, Z.; Li, Z.; Zhu, J.; Wang, Y.; Wu, L. Use of SAR/InSAR in Mining Deformation Monitoring, Parameter Inversion, and Forward Predictions: A Review. *IEEE Geosci. Remote Sens. Mag.* **2020**, *8*, 71–90. [[CrossRef](#)]
127. Talledo, D.A.; Miano, A.; Bonano, M.; Di Carlo, F.; Lanari, R.; Manunta, M.; Meda, A.; Mele, A.; Prota, A.; Saetta, A. Satellite radar interferometry: Potential and limitations for structural assessment and monitoring. *J. Build. Eng.* **2022**, *46*, 103756. [[CrossRef](#)]
128. Chen, Y.; Zhang, G.; Ding, X.; Li, Z. Monitoring earth surface deformations with InSAR technology: Principles and some critical issues. *J. Geospat. Eng.* **2000**, *2*, 3–22.
129. Gabriel, A.K.; Goldstein, R.M.; Zebker, H.A. Mapping small elevation changes over large areas: Differential radar interferometry. *J. Geophys. Res. Solid Earth* **1989**, *94*, 9183–9191. [[CrossRef](#)]
130. Massonnet, D.; Rossi, M.; Carmona, C.; Adragna, F.; Peltzer, G.; Feigl, K.; Rabaute, T. The displacement field of the Landers earthquake mapped by radar interferometry. *Nature* **1993**, *364*, 138–142. [[CrossRef](#)]
131. Massonnet, D.; Briole, P.; Arnaud, A. Deflation of Mount Etna monitored by spaceborne radar interferometry. *Nature* **1995**, *375*, 567–570. [[CrossRef](#)]
132. Crosetto, M.; Castillo, M.; Arbiol, R. Urban subsidence monitoring using radar interferometry. *Photogramm. Eng. Remote Sens.* **2003**, *69*, 775–783. [[CrossRef](#)]
133. Carnec, C.; Massonnet, D.; King, C. Two examples of the use of SAR interferometry on displacement fields of small spatial extent. *Geophys. Res. Lett.* **1996**, *23*, 3579–3582. [[CrossRef](#)]
134. Wang, C.; Zhang, H.; Liu, Z. ERS-1/2 SAR interferometry for urban subsidence detection in China. *ESA SP* **2000**, *461*, 2186–2191.
135. Carnec, C.; Raucoules, D. Assessment of SAR interferometry within operational application: Mapping and modelling of peri-urban subsidence. In Proceedings of the ESA-ENVISAT Symposium, Gothenburg, Sweden, 16–20 October 2000; Number SP-461.532. pp. 1–5.
136. Tesauro, M.; Bernardino, P.; Lanari, R.; Sansosti, E.; Fornaro, G.; Franceschetti, G. Urban subsidence inside the city of Napoli (Italy) observed by satellite radar interferometry. *Geophys. Res. Lett.* **2000**, *27*, 1961–1964. [[CrossRef](#)]
137. Cabral-Cano, E.; Dixon, T.; Sánchez, O. InSAR and GPS Analysis of Ground Subsidence in Mexico City. In Proceedings of the AGU Fall Meeting Abstracts, Washington, DC, USA, 2 August 2002; p. G61B-0980.
138. Thierry, P.; Deverly, F.; Reppelin, M.; Simonetto, E.; Lembezat, C.; Arnaud, A.; Raucoules, D.; Closset, L.; King, C. Survey of linear subsidence in an urban area using a 3D geological model and satellite Differential InSAR. In Proceedings of the Géoline Conference, Lyon, France, 23–25 May 2005.
139. Kim, J.-s.; Kim, D.-J.; Kim, S.-W.; Won, J.-S.; Moon, W.M. Monitoring of urban land surface subsidence using PSInSAR. *Geosci. J.* **2007**, *11*, 59–73. [[CrossRef](#)]
140. Stevens, N.F.; Glassey, P.; Lyttle, B.S. Slope Instability and Surface Deformation in Dunedin City, New Zealand. In Proceedings of the Envisat & ERS Symposium, Salzburg, Austria, 6–10 September 2004.
141. Werninghaus, R. TerraSAR-X mission. In *SAR Image Analysis, Modeling, and Techniques VI*; SPIE: Bellingham, WA, USA; pp. 9–16.
142. Virelli, M.; Coletta, A.; Battagliere, M.L. ASI COSMO-SkyMed: Mission overview and data exploitation. *IEEE Geosci. Remote Sens. Mag.* **2014**, *2*, 64–66. [[CrossRef](#)]
143. Eineder, M.; Adam, N.; Bamler, R.; Yague-Martinez, N.; Breit, H. Spaceborne spotlight SAR interferometry with TerraSAR-X. *IEEE Trans. Geosci. Remote Sens.* **2009**, *47*, 1524–1535. [[CrossRef](#)]
144. Farneti, E.; Cavalagli, N.; Costantini, M.; Trillo, F.; Minati, F.; Venanzi, I.; Ubertini, F. A method for structural monitoring of multispan bridges using satellite InSAR data with uncertainty quantification and its pre-collapse application to the Albiano-Magra Bridge in Italy. *Struct. Health Monit.* **2022**, *22*, 353–371. [[CrossRef](#)]
145. Wang, C.; Zhang, Z.; Zhang, H.; Wu, Q.; Zhang, B.; Tang, Y. Seasonal deformation features on Qinghai-Tibet railway observed using time-series InSAR technique with high-resolution TerraSAR-X images. *Remote Sens. Lett.* **2017**, *8*, 1–10. [[CrossRef](#)]
146. Zhang, B.; Liao, X.; Zhang, J.; Xiong, S.; Wang, C.; Wu, S.; Zhu, C.; Qin, X.; Li, Q. Megalopolitan-scale ground deformation along metro lines in the Guangdong-Hong Kong-Macao Greater Bay Area, China, revealed by MT-InSAR. *Int. J. Appl. Earth Obs. Geoinf.* **2023**, *122*, 103432. [[CrossRef](#)]
147. Yu, B.; Liu, G.; Zhang, R.; Jia, H.; Li, T.; Wang, X.; Dai, K.; Ma, D. Monitoring subsidence rates along road network by persistent scatterer SAR interferometry with high-resolution TerraSAR-X imagery. *J. Mod. Transp.* **2013**, *21*, 236–246. [[CrossRef](#)]
148. Xie, L.; Xu, W.; Ding, X. Precursory motion and deformation mechanism of the 2018 Xe Pian-Xe Namnoy dam Collapse, Laos: Insights from satellite radar interferometry. *Int. J. Appl. Earth Obs. Geoinf.* **2022**, *109*, 102797. [[CrossRef](#)]
149. Attema, E.; Davidson, M.; Snoeij, P.; Rommen, B.; Floury, N. Sentinel-1 mission overview. In Proceedings of the 2009 IEEE International Geoscience and Remote Sensing Symposium, Cape Town, South Africa, 12–17 July 2009; pp. I-36–I-39.
150. Frantz, D.; Schug, F.; Okujeni, A.; Navacchi, C.; Wagner, W.; van der Linden, S.; Hostert, P. National-scale mapping of building height using Sentinel-1 and Sentinel-2 time series. *Remote Sens. Environ.* **2021**, *252*, 112128. [[CrossRef](#)] [[PubMed](#)]
151. Novellino, A.; Cigna, F.; Brahmi, M.; Sowter, A.; Bateson, L.; Marsh, S. Assessing the feasibility of a national InSAR ground deformation map of Great Britain with Sentinel-1. *Geosciences* **2017**, *7*, 19. [[CrossRef](#)]
152. Crosetto, M.; Monserrat, O.; Luzi, G.; Cuevas, M.; Devanthery, N. Deformation monitoring using ground-based SAR data. In *Engineering Geology for Society and Territory-Volume 5: Urban Geology, Sustainable Planning and Landscape Exploitation*; Springer: Berlin/Heidelberg, Germany, 2015; pp. 137–140.

153. Noferini, L.; Mecatti, D.; Macaluso, G.; Pieraccini, M.; Atzeni, C. Monitoring of Belvedere Glacier using a wide angle GB-SAR interferometer. *J. Appl. Geophys.* **2009**, *68*, 289–293. [[CrossRef](#)]
154. Dick, G.J.; Eberhardt, E.; Cabrejo-Liévano, A.G.; Stead, D.; Rose, N.D. Development of an early-warning time-of-failure analysis methodology for open-pit mine slopes utilizing ground-based slope stability radar monitoring data. *Can. Geotech. J.* **2015**, *52*, 515–529. [[CrossRef](#)]
155. Wang, Y.; Hong, W.; Zhang, Y.; Lin, Y.; Li, Y.; Bai, Z.; Zhang, Q.; Lv, S.; Liu, H.; Song, Y. Ground-based differential interferometry SAR: A review. *IEEE Geosci. Remote Sens. Mag.* **2020**, *8*, 43–70. [[CrossRef](#)]
156. Luzi, G.; Crosetto, M. Building monitoring using a ground-based radar. In *Encyclopedia of Earthquake Engineering*; Springer: Berlin/Heidelberg, Germany, 2014.
157. Feng, W.; Friedt, J.-M.; Nico, G.; Wang, S.; Martin, G.; Sato, M. Passive bistatic ground-based synthetic aperture radar: Concept, system, and experiment results. *Remote Sens.* **2019**, *11*, 1753. [[CrossRef](#)]
158. Scaioni, M.; Wang, J. Technologies for Dam Deformation Measurement: Recent Trends and Future Challenges. In Proceedings of the 3rd Joint Int. Symp. on Deformation Monitoring, Vienna, Austria, 30 March–1 April 2016; pp. 1–8.
159. Zhang, B.; Ding, X.; Werner, C.; Tan, K.; Zhang, B.; Jiang, M.; Zhao, J.; Xu, Y. Dynamic displacement monitoring of long-span bridges with a microwave radar interferometer. *ISPRS J. Photogramm. Remote Sens.* **2018**, *138*, 252–264. [[CrossRef](#)]
160. Michel, C.; Keller, S. Advancing ground-based radar processing for bridge infrastructure monitoring. *Sensors* **2021**, *21*, 2172. [[CrossRef](#)]
161. Zhao, Z.; Deng, Y.; Tian, W.; Hu, C.; Lin, Z.; Zeng, T. Dynamic Deformation Measurement of Bridge Structure Based on GB-MIMO Radar. *IEEE Trans. Geosci. Remote Sens.* **2022**, *60*, 4708314. [[CrossRef](#)]
162. Huang, Q.; Wang, Y.; Luzi, G.; Crosetto, M.; Monserrat, O.; Jiang, J.; Zhao, H.; Ding, Y. Ground-based radar interferometry for monitoring the dynamic performance of a multitrack steel truss high-speed railway bridge. *Remote Sens.* **2020**, *12*, 2594. [[CrossRef](#)]
163. Serrano-Juan, A.; Vázquez-Suñé, E.; Monserrat, O.; Crosetto, M.; Hoffmann, C.; Ledesma, A.; Criollo, R.; Pujades, E.; Velasco, V.; Garcia-Gil, A. Gb-SAR interferometry displacement measurements during dewatering in construction works. Case of La Sagrera railway station in Barcelona, Spain. *Eng. Geol.* **2016**, *205*, 104–115. [[CrossRef](#)]
164. Montuori, A.; Luzi, G.; Bignami, C.; Gaudiosi, I.; Stramondo, S.; Crosetto, M.; Buongiorno, F. A Non-Invasive Methodology for the Urban Monitoring Based on the Combined Use of InSAR, GBSAR and RAR Sensors: From the Surface Deformations to Single-Building Dynamical Behaviour. In Proceedings of the Living Planet Symposium, Prague, Czech Republic, 9–13 May 2016; p. 396.
165. Rebmeister, M.; Auer, S.; Schenk, A.; Hinz, S. Geocoding of ground-based SAR data for infrastructure objects using the Maximum A Posteriori estimation and ray-tracing. *ISPRS J. Photogramm. Remote Sens.* **2022**, *189*, 110–127. [[CrossRef](#)]
166. Tapete, D.; Casagli, N.; Luzi, G.; Fanti, R.; Gigli, G.; Leva, D. Integrating radar and laser-based remote sensing techniques for monitoring structural deformation of archaeological monuments. *J. Archaeol. Sci.* **2013**, *40*, 176–189. [[CrossRef](#)]
167. Zhu, Y.; Xu, B.; Li, Z.; Hou, J.; Wang, Q. Monitoring bridge vibrations based on GBSAR and validation by high-rate GPS measurements. *IEEE J. Sel. Top. Appl. Earth Obs. Remote Sens.* **2021**, *14*, 5572–5580. [[CrossRef](#)]
168. Kačan, M.; Turčinović, F.; Bojanjac, D.; Bosiljevac, M. Deep Learning Approach for Object Classification on Raw and Reconstructed GBSAR Data. *Remote Sens.* **2022**, *14*, 5673. [[CrossRef](#)]
169. Liu, G.; Jia, H.; Zhang, R.; Zhang, H.; Jia, H.; Yu, B.; Sang, M. Exploration of subsidence estimation by persistent scatterer InSAR on time series of high resolution TerraSAR-X images. *IEEE J. Sel. Top. Appl. Earth Obs. Remote Sens.* **2010**, *4*, 159–170. [[CrossRef](#)]
170. Wu, S.; Zhang, B.; Liang, H.; Wang, C.; Ding, X.; Zhang, L. Detecting the Deformation Anomalies Induced by Underground Construction Using Multiplatform MT-InSAR: A Case Study in To Kwa Wan Station, Hong Kong. *IEEE J. Sel. Top. Appl. Earth Obs. Remote Sens.* **2021**, *14*, 9803–9814. [[CrossRef](#)]
171. Zhang, B.; Wu, S.; Ding, X.; Wang, C.; Zhu, J.; Li, Q. Use of Multiplatform SAR Imagery in Mining Deformation Monitoring with Dense Vegetation Coverage: A Case Study in the Fengfeng Mining Area, China. *Remote Sens.* **2021**, *13*, 3091. [[CrossRef](#)]
172. Hu, C.; Deng, Y.; Wang, R.; Tian, W.; Zeng, T. Two-dimensional deformation measurement based on multiple aperture interferometry in GB-SAR. *IEEE Geosci. Remote Sens. Lett.* **2016**, *14*, 208–212. [[CrossRef](#)]
173. Deng, Y.; Hu, C.; Tian, W.; Zhao, Z. 3-D deformation measurement based on three GB-MIMO radar systems: Experimental verification and accuracy analysis. *IEEE Geosci. Remote Sens. Lett.* **2020**, *18*, 2092–2096. [[CrossRef](#)]
174. Monti-Guarnieri, A.; Falcone, P.; d’Aria, D.; Giunta, G. 3D vibration estimation from ground-based radar. *Remote Sens.* **2018**, *10*, 1670. [[CrossRef](#)]
175. Miccinesi, L.; Pieraccini, M. Bridge monitoring by a monostatic/bistatic interferometric radar able to retrieve the dynamic 3D displacement vector. *IEEE Access* **2020**, *8*, 210339–210346. [[CrossRef](#)]
176. Crosetto, M.; Monserrat, O.; Cuevas-González, M.; Devanthéry, N.; Luzi, G.; Crippa, B. Measuring thermal expansion using X-band persistent scatterer interferometry. *ISPRS J. Photogramm. Remote Sens.* **2015**, *100*, 84–91. [[CrossRef](#)]
177. Monserrat, O.; Crosetto, M.; Cuevas, M.; Crippa, B. The thermal expansion component of persistent scatterer interferometry observations. *IEEE Geosci. Remote Sens. Lett.* **2011**, *8*, 864–868. [[CrossRef](#)]
178. Ma, P.; Lin, H.; Lan, H.; Chen, F. Multi-dimensional SAR tomography for monitoring the deformation of newly built concrete buildings. *ISPRS J. Photogramm. Remote Sens.* **2015**, *106*, 118–128. [[CrossRef](#)]
179. Li, Z.; Cao, Y.; Wei, J.; Duan, M.; Wu, L.; Hou, J.; Zhu, J. Time-series InSAR ground deformation monitoring: Atmospheric delay modeling and estimating. *Earth-Sci. Rev.* **2019**, *192*, 258–284. [[CrossRef](#)]

180. Farshbaf, A.; Mousavi, M.N.; Shahnazi, S. Vulnerability assessment of power transmission towers affected by land subsidence via interferometric synthetic aperture radar technique and finite element method analysis: A case study of Zanjan and Qazvin provinces. *Environ. Dev. Sustain.* **2023**, 1–20. [[CrossRef](#)]
181. Bozzano, F.; Esposito, C.; Franchi, S.; Mazzanti, P.; Perissin, D.; Rocca, A.; Romano, E. Analysis of a subsidence process by integrating geological and hydrogeological modelling with satellite InSAR Data. In *Engineering Geology for Society and Territory-Volume 5: Urban Geology, Sustainable Planning and Landscape Exploitation*; Springer: Berlin/Heidelberg, Germany, 2015; pp. 155–159.
182. Du, Y.; Zhang, L.; Feng, G.; Lu, Z.; Sun, Q. On the accuracy of topographic residuals retrieved by MTInSAR. *IEEE Trans. Geosci. Remote Sens.* **2017**, *55*, 1053–1065. [[CrossRef](#)]
183. Montazeri, S.; Rodríguez González, F.; Zhu, X. Geocoding Error Correction for InSAR Point Clouds. *Remote Sens.* **2018**, *10*, 1523. [[CrossRef](#)]
184. Zhu, X.X.; Bamler, R. Superresolving SAR tomography for multidimensional imaging of urban areas: Compressive sensing-based TomoSAR inversion. *IEEE Signal Process. Mag.* **2014**, *31*, 51–58. [[CrossRef](#)]
185. Wang, Y.; Zhu, X.X. Automatic feature-based geometric fusion of multiview TomoSAR point clouds in urban area. *IEEE J. Sel. Top. Appl. Earth Obs. Remote Sens.* **2014**, *8*, 953–965. [[CrossRef](#)]
186. Wang, Y.; Zhu, X.X.; Bamler, R. Retrieval of phase history parameters from distributed scatterers in urban areas using very high resolution SAR data. *ISPRS J. Photogramm. Remote Sens.* **2012**, *73*, 89–99. [[CrossRef](#)]
187. Lombardini, F.; Cai, F. Generalized-Capon method for Diff-Tomo SAR analyses of decorrelating scatterers. *Remote Sens.* **2019**, *11*, 412. [[CrossRef](#)]
188. Cai, J.; Jia, H.; Liu, G.; Zhang, B.; Liu, Q.; Fu, Y.; Wang, X.; Zhang, R. An accurate geocoding method for gb-sar images based on solution space search and its application in landslide monitoring. *Remote Sens.* **2021**, *13*, 832. [[CrossRef](#)]
189. Montuori, A.; Luzi, G.; Stramondo, S.; Casula, G.; Bignami, C.; Bonali, E.; Bianchi, M.G.; Crosetto, M. Combined use of ground-based systems for Cultural Heritage conservation monitoring. In Proceedings of the 2014 IEEE Geoscience and Remote Sensing Symposium, Quebec City, QC, Canada, 13–18 July 2014; pp. 4086–4089.
190. Hu, C.; Deng, Y.; Tian, W. *Multistatic Ground-Based Differential Interferometric MIMO Radar for 3D Deformation Measurement*; Science China Press Beijing: Beijing, China, 2021.
191. Zhu, W.; Li, W.-L.; Zhang, Q.; Yang, Y.; Zhang, Y.; Qu, W.; Wang, C.-S. A decade of ground deformation in Kunming (China) revealed by multi-temporal synthetic aperture radar interferometry (InSAR) technique. *Sensors* **2019**, *19*, 4425. [[CrossRef](#)]
192. Wu, S.; Yang, Z.; Ding, X.; Zhang, B.; Zhang, L.; Lu, Z. Two Decades of Settlement of Hong Kong International Airport Measured with Multi-Temporal InSAR. *Remote Sens. Environ.* **2020**, *248*, 111976. [[CrossRef](#)]
193. Li, G.; Zhao, C.; Wang, B.; Peng, M.; Bai, L. Evolution of spatiotemporal ground deformation over 30 years in Xi'an, China, with multi-sensor SAR interferometry. *J. Hydrol.* **2023**, *616*, 128764. [[CrossRef](#)]
194. Zhu, M.; Wan, X.; Fei, B.; Qiao, Z.; Ge, C.; Minati, F.; Vecchioli, F.; Li, J.; Costantini, M. Detection of Building and Infrastructure Instabilities by Automatic Spatiotemporal Analysis of Satellite SAR Interferometry Measurements. *Remote Sens.* **2018**, *10*, 1816. [[CrossRef](#)]
195. Macchiarulo, V.; Milillo, P.; Blenkinsopp, C.; Giardina, G. Monitoring deformations of infrastructure networks: A fully automated GIS integration and analysis of InSAR time-series. *Struct. Health Monit.* **2022**, *21*, 1849–1878. [[CrossRef](#)]
196. Malik, K.; Kumar, D.; Perissin, D.; Pradhan, B. Estimation of ground subsidence of New Delhi, India using PS-InSAR technique and Multi-sensor Radar data. *Adv. Space Res.* **2022**, *69*, 1863–1882. [[CrossRef](#)]
197. Sharma, J.; Eppler, J.; Busler, J. Urban infrastructure monitoring with a spatially adaptive multi-looking InSAR technique. *Proc. Fringe Frascati Italy* **2015**, *731*, 64. [[CrossRef](#)]
198. Yang, M.; Yang, T.; Zhang, L.; Lin, J.; Qin, X.; Liao, M. Spatio-temporal characterization of a reclamation settlement in the Shanghai coastal area with time series analyses of X-, C-, and L-band SAR datasets. *Remote Sens.* **2018**, *10*, 329. [[CrossRef](#)]
199. Liu, X.; Wang, P.; Lu, Z.; Gao, K.; Wang, H.; Jiao, C.; Zhang, X. Damage detection and analysis of urban bridges using terrestrial laser scanning (TLS), ground-based microwave interferometry, and permanent scatterer interferometry synthetic aperture radar (PS-InSAR). *Remote Sens.* **2019**, *11*, 580. [[CrossRef](#)]
200. Costantini, M.; Minati, F.; Trillo, F.; Ferretti, A.; Novali, F.; Passera, E.; Dehls, J.; Larsen, Y.; Marinkovic, P.; Eineder, M. European ground motion service (EGMS). In Proceedings of the 2021 IEEE International Geoscience and Remote Sensing Symposium IGARSS, Brussels, Belgium, 11–16 July 2021; pp. 3293–3296.
201. Chang, L.; Hanssen, R.F. Detection of cavity migration and sinkhole risk using radar interferometric time series. *Remote Sens. Environ.* **2014**, *147*, 56–64. [[CrossRef](#)]
202. Li, T.; Motagh, M.; Wang, M.; Zhang, W.; Gong, C.; Xiong, X.; He, J.; Chen, L.; Liu, J. Earth and rock-filled dam monitoring by high-resolution X-band interferometry: Gongming dam case study. *Remote Sens.* **2019**, *11*, 246. [[CrossRef](#)]
203. Emadali, L.; Motagh, M.; Haghghi, M.H. Characterizing post-construction settlement of the Masjed-Soleyman embankment dam, Southwest Iran, using TerraSAR-X SpotLight radar imagery. *Eng. Struct.* **2017**, *143*, 261–273. [[CrossRef](#)]
204. Qin, X.; Li, Q.; Ding, X.; Xie, L.; Wang, C.; Liao, M.; Zhang, L.; Zhang, B.; Xiong, S. A structure knowledge-synthetic aperture radar interferometry integration method for high-precision deformation monitoring and risk identification of sea-crossing bridges. *Int. J. Appl. Earth Obs. Geoinf.* **2021**, *103*, 102476. [[CrossRef](#)]

205. Lu, Z.; Dzurisin, D. InSAR Imaging of Aleutian Volcanoes. In *InSAR Imaging of Aleutian Volcanoes: Monitoring a Volcanic Arc from Space*; Springer: Berlin/Heidelberg, Germany, 2014; pp. 87–345.
206. Budillon, A.; Crosetto, M.; Johnsy, A.C.; Monserrat, O.; Krishnakumar, V.; Schirinzi, G. Comparison of persistent scatterer interferometry and SAR tomography using Sentinel-1 in urban environment. *Remote Sens.* **2018**, *10*, 1986. [[CrossRef](#)]
207. Tian, Z.; Fan, H.; Cao, F.; He, L. Monitoring Surface Subsidence Using Distributed Scatterer InSAR with an Improved Statistically Homogeneous Pixel Selection Method in Coalfield Fire Zones. *Remote Sens.* **2023**, *15*, 3574. [[CrossRef](#)]
208. Fadhillah, M.F.; Achmad, A.R.; Lee, C.-W. Improved combined scatterers interferometry with optimized point scatterers (ICOPS) for interferometric synthetic aperture radar (InSAR) time-series analysis. *IEEE Trans. Geosci. Remote Sens.* **2021**, *60*, 5220014. [[CrossRef](#)]
209. Hussain, E.; Hooper, A.; Wright, T.J.; Walters, R.J.; Bekaert, D.P. Interseismic strain accumulation across the central North Anatolian Fault from iteratively unwrapped InSAR measurements. *J. Geophys. Res. Solid Earth* **2016**, *121*, 9000–9019. [[CrossRef](#)]
210. Yu, H.; Lan, Y.; Yuan, Z.; Xu, J.; Lee, H. Phase unwrapping in InSAR: A review. *IEEE Geosci. Remote Sens. Mag.* **2019**, *7*, 40–58. [[CrossRef](#)]
211. Ansari, H.; De Zan, F.; Bamler, R. Sequential Estimator: Toward Efficient InSAR Time Series Analysis. *IEEE Trans. Geosci. Remote Sens.* **2017**, *55*, 5637–5652. [[CrossRef](#)]
212. Shi, G.; Lin, H.; Ma, P. A hybrid method for stability monitoring in low-coherence urban regions using persistent and distributed scatterers. *IEEE J. Sel. Top. Appl. Earth Obs. Remote Sens.* **2018**, *11*, 3811–3821. [[CrossRef](#)]
213. Shi, G.; Lin, H.; Bürgmann, R.; Ma, P.; Wang, J.; Liu, Y. Early soil consolidation from magnetic extensometers and full resolution SAR interferometry over highly decorrelated reclaimed lands. *Remote Sens. Environ.* **2019**, *231*, 111231. [[CrossRef](#)]
214. Morishita, Y.; Hanssen, R.F. Deformation parameter estimation in low coherence areas using a multisatellite InSAR approach. *IEEE Trans. Geosci. Remote Sens.* **2015**, *53*, 4275–4283. [[CrossRef](#)]
215. Ottavianelli, G.; Hobbs, S.E.; Bruno, D.; Smith, R. Earth Observation for Solid Waste Landfill Managem. In Proceedings of the 56th International Astronautical Congress of the International Astronautical Federation, the International Academy of Astronautics, and the International Institute of Space Law, Fukuoka, Japan, 17–21 October 2005; p. B1. 5.01.
216. Stabile, T.A.; Perrone, A.; Gallipoli, M.R.; Ditommaso, R.; Ponzio, F.C. Dynamic survey of the Musmeci bridge by joint application of ground-based microwave radar interferometry and ambient noise standard spectral ratio techniques. *IEEE Geosci. Remote Sens. Lett.* **2013**, *10*, 870–874. [[CrossRef](#)]
217. Dörr, N.; Schenk, A.; Hinz, S. Fully Integrated Temporary Persistent Scatterer Interferometry. *IEEE Trans. Geosci. Remote Sens.* **2022**, *60*, 4412815. [[CrossRef](#)]
218. Wang, B.; Zhao, C.; Zhang, Q.; Lu, Z.; Li, Z.; Liu, Y. Sequential estimation of dynamic deformation parameters for SBAS-InSAR. *IEEE Geosci. Remote Sens. Lett.* **2019**, *17*, 1017–1021. [[CrossRef](#)]
219. Crosetto, M.; Monserrat, O.; Luzi, G.; Cuevas-González, M.; Devanthery, N. Discontinuous GBSAR deformation monitoring. *ISPRS J. Photogramm. Remote Sens.* **2014**, *93*, 136–141. [[CrossRef](#)]
220. Anantrasirichai, N.; Biggs, J.; Albino, F.; Hill, P.; Bull, D. Application of machine learning to classification of volcanic deformation in routinely generated InSAR data. *J. Geophys. Res. Solid Earth* **2018**, *123*, 6592–6606. [[CrossRef](#)]
221. Wu, Z.; Ma, P.; Zheng, Y.; Gu, F.; Liu, L.; Lin, H. Automatic detection and classification of land subsidence in deltaic metropolitan areas using distributed scatterer InSAR and Oriented R-CNN. *Remote Sens. Environ.* **2023**, *290*, 113545. [[CrossRef](#)]

Disclaimer/Publisher’s Note: The statements, opinions and data contained in all publications are solely those of the individual author(s) and contributor(s) and not of MDPI and/or the editor(s). MDPI and/or the editor(s) disclaim responsibility for any injury to people or property resulting from any ideas, methods, instructions or products referred to in the content.